




RESEARCH ARTICLE

10.1002/2017MS001028

Modeling CO₂ emissions from Arctic lakes: Model development and site-level studyZeli Tan^{1,2} , Qianlai Zhuang^{1,3} , Narasinha J. Shurpali⁴ , Maija E. Marushchak⁴, Christina Biasi⁴ , Werner Eugster⁵ , and Katey Walter Anthony⁶

Key Points:

- The ALBM reproduces CO₂ fluxes from different Arctic lakes
- The model can simulate the carbon balance of Arctic lakes, a difficult task for field and lab experiments and other biogeochemistry models
- The contribution of glacial lakes to the global carbon cycle could be the largest because of their much larger surface area and high fluxes

Supporting Information:

- Supporting Information S1

Correspondence to:

Q. Zhuang,
qzhuang@purdue.edu

Citation:

Tan, Z., Q. Zhuang, N. J. Shurpali, M. E. Marushchak, C. Biasi, W. Eugster, and K. W. Anthony (2017), Modeling CO₂ emissions from Arctic lakes: Model development and site-level study, *J. Adv. Model. Earth Syst.*, 9, doi:10.1002/2017MS001028.

Received 23 APR 2017

Accepted 29 AUG 2017

Accepted article online 2 SEP 2017

¹Department of Earth, Atmospheric, and Planetary Sciences, Purdue University, West Lafayette, Indiana, USA, ²Now at Pacific Northwest National Laboratory, Richland, Washington, USA, ³Department of Agronomy, Purdue University, West Lafayette, Indiana, USA, ⁴Department of Environmental and Biological Science, University of Eastern Finland, Kuopio, Finland, ⁵Department of Environmental Systems Science, ETH Zurich, Zurich, Switzerland, ⁶Water and Environmental Research Center, University of Alaska Fairbanks, Fairbanks, Alaska, USA

Abstract Recent studies indicated that Arctic lakes play an important role in receiving, processing, and storing organic carbon exported from terrestrial ecosystems. To quantify the contribution of Arctic lakes to the global carbon cycle, we developed a one-dimensional process-based Arctic Lake Biogeochemistry Model (ALBM) that explicitly simulates the dynamics of organic and inorganic carbon in Arctic lakes. By realistically modeling water mixing, carbon biogeochemistry, and permafrost carbon loading, the model can reproduce the seasonal variability of CO₂ fluxes from the study Arctic lakes. The simulated area-weighted CO₂ fluxes from yedoma thermokarst lakes, nonyedoma thermokarst lakes, and glacial lakes are 29.5, 13.0, and 21.4 g C m⁻² yr⁻¹, respectively, close to the observed values (31.2, 17.2, and 16.5 ± 7.7 g C m⁻² yr⁻¹, respectively). The simulations show that the high CO₂ fluxes from yedoma thermokarst lakes are stimulated by the biomineralization of mobilized labile organic carbon from thawing yedoma permafrost. The simulations also imply that the relative contribution of glacial lakes to the global carbon cycle could be the largest because of their much larger surface area and high biomineralization and carbon loading. According to the model, sunlight-induced organic carbon degradation is more important for shallow nonyedoma thermokarst lakes but its overall contribution to the global carbon cycle could be limited. Overall, the ALBM can simulate the whole-lake carbon balance of Arctic lakes, a difficult task for field and laboratory experiments and other biogeochemistry models.

Plain Language Summary Few lake biogeochemistry models are developed specifically for Arctic lakes which are found to be important in understanding the global carbon cycle. In this study, we developed a one-dimensional process-based lake biogeochemistry model that explicitly simulates the dynamics of organic and inorganic carbon in Arctic lakes. By realistically modeling water mixing, carbon biogeochemistry, and permafrost carbon loading, the model can reproduce the seasonal variability of CO₂ fluxes from the study Arctic lakes. The simulations show that for the global carbon cycle the relative contribution of glacial lakes could be the largest because of their much larger surface area and high carbon oxidation and loading, and the overall contribution of sunlight-induced organic carbon oxidation is limited due to the limitation of UV energy. Importantly, this lake model can simulate the whole-lake carbon balance of Arctic lakes, a difficult task for field and laboratory experiments and other biogeochemistry models.

© 2017. The Authors.

This is an open access article under the terms of the Creative Commons Attribution-NonCommercial-NoDerivs License, which permits use and distribution in any medium, provided the original work is properly cited, the use is non-commercial and no modifications or adaptations are made.

1. Introduction

Inland waters (e.g., lakes, rivers, and streams) are regulators of global carbon cycling and climate [Tranvik *et al.*, 2009]. Approximately, 1.9 pg C yr⁻¹ of soil carbon enters inland waters where it is processed, out-gassed, and deposited such that only ~0.9 pg C yr⁻¹ is exported to the coastal ocean [Cole *et al.*, 2007]. Recent studies indicated that Arctic lakes could have significant impacts on the global carbon cycle [Walter *et al.*, 2006; Walter Anthony *et al.*, 2014; Tan *et al.*, 2016; Wik *et al.*, 2016]. First, lakes are a prominent landscape in the Arctic [Downing *et al.*, 2006; Verpoorter *et al.*, 2014]. They cover over 12.5% of the coastal lowlands in northern Canada and northeastern Siberia [Paltan *et al.*, 2015] and 40–80% (including marshes) of

the area near the coast of northern Alaska [Kling *et al.*, 1991]. Second, the amount of soil organic carbon (SOC) exported annually to the lakes and rivers in the pan-Arctic can be more than 10% of the regional net ecosystem production of terrestrial ecosystems [Weyhenmeyer *et al.*, 2012]. Third, due to the release of very labile organic carbon (OC) from thawing pan-Arctic permafrost [Tarnocai *et al.*, 2009; Vonk *et al.*, 2013; Spencer *et al.*, 2015; Drake *et al.*, 2015], the microbial production of carbon dioxide (CO₂) and methane (CH₄) in Arctic lakes and rivers will likely increase rapidly in the future. Fourth, in the pan-Arctic small thermokarst lakes and ponds, especially yedoma lakes are found to emit more CO₂ and CH₄ per unit area than the surrounding landscapes [Langer *et al.*, 2015; Sepulveda-Jauregui *et al.*, 2015]; however, the underlying mechanism is not yet fully understood [Walter *et al.*, 2006; Walter Anthony *et al.*, 2014; Stackpoole *et al.*, 2017].

Field investigations suggested that the carbon dynamics in Arctic lakes involve complex interactions among different physical and biogeochemical processes (e.g., convective mixing and carbon fixation) and are influenced substantially by the local environment (e.g., permafrost) and lake characteristics (e.g., lake size and depth). For example, while photochemical degradation usually accounts for a minor fraction of DOC loss in the water column of lakes in other climate zones [Bertilsson and Tranvik, 2000; Groeneveld *et al.*, 2016], it was found to contribute up to 95% of DOC loss in some Arctic lakes [Cory *et al.*, 2014]. In addition to oxidizing DOC directly to inorganic forms (e.g., CO₂), sunlight can alter the rate of DOC degradation indirectly by producing free radicals and reactive oxygen (O₂) species [Burd *et al.*, 2015] and fueling microbial degradation [Cory *et al.*, 2014]. The increased DOC export from the permafrost region can cause carbon and nutrient enrichment in Arctic lakes [Walter Anthony *et al.*, 2014]. The effects of this enrichment on the carbon dynamics are complex [Daniels *et al.*, 2015; Seekell *et al.*, 2015]. Some studies suggested that it would stimulate primary production, CO₂ and CH₄ production, and OC burial [Sobek *et al.*, 2009; Walter Anthony *et al.*, 2014]. It was also found to reduce water transparency, stimulate water stratification, and increase O₂ deficit in the bottom waters and sediments [Daniels *et al.*, 2015; Deshpande *et al.*, 2015]. In addition to permafrost thawing, rapid warming in the Arctic is causing the reduction of lake convective mixing and ice cover periods [O'Reilly *et al.*, 2015; Arp *et al.*, 2016], two important factors for carbon outgassing [Eugster *et al.*, 2003; Greene *et al.*, 2014]. Consequently, the phytoplankton species in Arctic lakes may need to adapt to the new environment for survival [Rousseaux and Gregg, 2015]. Obviously, these complex interactions make it difficult to evaluate the carbon dynamics of Arctic lakes at large spatial scales without a process-based lake biogeochemistry model [Aufdenkampe *et al.*, 2011; Stepanenko *et al.*, 2016]. Further, the lack of such a modeling tool also impedes a complete landscape-scale assessment of the carbon budget in the pan-Arctic involving aquatic systems, as Buffam *et al.* [2011] did for a north temperate region.

Here we developed a one-dimensional (1-D) process-based Arctic Lake Biogeochemistry Model (ALBM) and evaluated it with observations from six representative Arctic lakes, including yedoma thermokarst lakes (formed in the Pleistocene-aged, organic-rich ice complex known as “yedoma,” herein yedoma lakes), non-yedoma thermokarst lakes (formed in nonyedoma permafrost soils, herein thermokarst lakes), and glacial lakes (formed through the glacial activity during the past ice ages). The ALBM is based on the lake biogeochemistry model (bLake4Me) for simulating CH₄ production, oxidation, and emission in Arctic lakes [Tan *et al.*, 2015]. To estimate the carbon dynamics in lake waters and sediments, we include several processes that account for carbon fixation and metabolic carbon loss by phytoplankton, carbon mineralization by microbes, sunlight-induced photochemical mineralization, and terrigenous carbon transport. A solar radiation transfer model is integrated to simulate the available radiation for photosynthesis and photomineralization in lake waters. Section 2 describes the details of the carbon cycle model (section 2.1.1), the solar radiation transfer model (section 2.1.2), and the changes to other components of the bLake4Me model (section 2.1.3). Section 2 also describes the observations and driving data to evaluate the ALBM (section 2.2.1) and the methods for model sensitivity analysis and model calibration (section 2.2.2). Section 3 discusses the results of model sensitivity analysis and evaluation. Section 4 discusses the limitations of the study and section 5 summarizes the key findings. By using the ALBM, we aim to explain the spatial and temporal variability of the carbon dynamics in Arctic lakes, such as high CO₂ fluxes and phytoplankton primary production in spring and fall seasons driven by convective mixing, and high CO₂ fluxes from yedoma lakes driven by the release of labile OC from thawing permafrost. The findings are discussed from a viewpoint of climate change.

2. Methods

2.1. Model Description

We upgraded the lake biogeochemistry model (bLake4Me) introduced by *Tan et al.* [2015] to improve our understanding of the carbon dynamics in pan-Arctic lakes. *Tan et al.* [2015] showed that the bLake4Me model can reproduce the thermal and CH₄ dynamics in the water and sediment columns of both yedoma and glacial lakes. To further simulate the CO₂ dynamics in Arctic lakes, we added several new modules to the ALBM (Figure 1), including the loading of OC from terrestrial ecosystems, the microbial and photochemical degradation of OC, the fixation of inorganic carbon by photosynthesis, and the loss of phytoplankton biomass by respiration, exudation, and mortality. The ALBM has several features that are important for understanding the carbon dynamics in Arctic lakes but are lacking in other lake models, including (1) simulates the thawing and freezing cycles of sediments in thermokarst lakes; (2) simulates the mobilization and mineralization of labile OC in the deep sediments of yedoma lakes; (3) represents the OC inputs induced by thermokarst activities; and (4) simulates the degradation of DOC by photochemical mineralization.

2.1.1. Carbon Cycle Model

The carbon cycle model was designed to quantify the flow of carbon and nutrients in the water and sediment columns of Arctic lakes. The flow of carbon includes inorganic carbon fixation, OC mineralization and deposition, CH₄ oxidation, CO₂ and CH₄ outgassing, and the load of organic and inorganic carbon through surface and subsurface water flow and permafrost thawing. The flow of nutrients includes nutrient assimilation through photosynthesis, nutrient mobilization through OC mineralization, and the load of nutrients through surface and subsurface water flow. By assuming phosphorus as the major element responsible for nutrient limitation of phytoplankton primary production [*Hanson et al.*, 2004; *Jäger and Diehl*, 2014], we assign carbon substances into three pools (DIC, DOC, and POC), and phosphorus substances into a single inorganic pool (SRP: soluble reactive phosphorus). The DIC pool includes three forms of dissolved CO₂ in

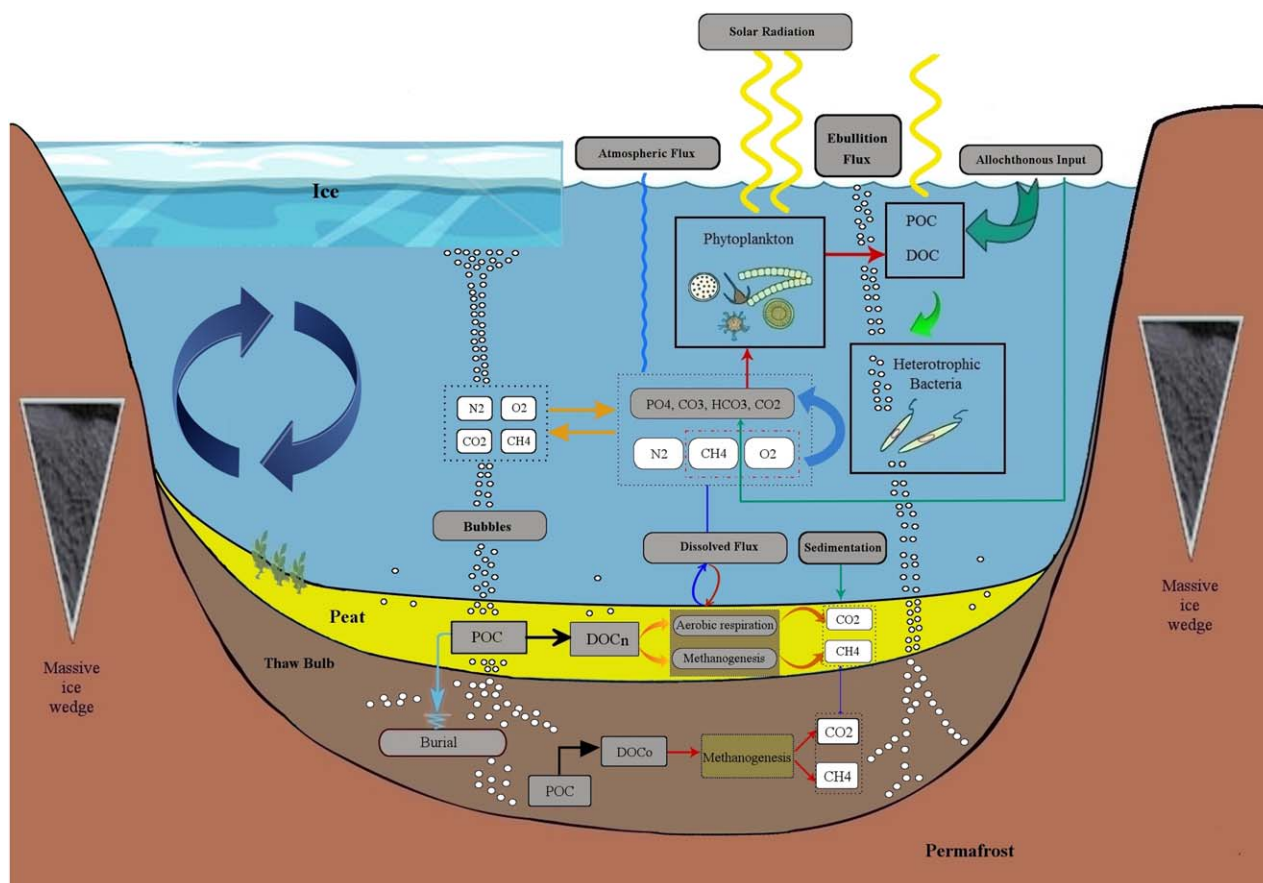


Figure 1. Simplified schematic of carbon and nutrient dynamics in the ALBM.

water: aqueous CO₂, bicarbonate (HCO₃⁻), and carbonate (CO₃²⁻). There are two DOC pools (*DOC_{tr}* and *DOC_{aq}*) for terrestrially and aquatically derived DOC, respectively, which are different in recalcitrance and optical properties. The *DOC_{aq}* pool is increased by phytoplankton primary production and the *DOC_{tr}* pool is increased by land carbon export (e.g., carbon fluxes through surface and subsurface water flow) and dry and wet carbon deposition. We define two phytoplankton functional types: small-size (e.g., cyanobacteria) and large-size (e.g., diatoms) phytoplankton, accounting for the variation in biological traits within the community [Wetzel, 2001; Wang et al., 2009]. In general, diatoms have high growth and large sinking rates, allowing them to flourish in nutrient and light rich areas but preventing them from dominating in quiescent regions [Rousseaux and Gregg, 2015]. In contrast, cyanobacteria have low growth and sinking rates and can sustain in nutrient-poor and windless areas [Rousseaux and Gregg, 2015]. For small, cold, and nutrient-poor Arctic lakes, small phytoplankton has dominance in community composition [Sheath, 1986]. The organic forms of phosphorus are cycled firmly at fixed C:P stoichiometry quotients with the pools of POC and DOC.

As described by Tan and Zhuang [2015a], the 1-D water column is divided into a number of layers: (1) for shallow lakes less than 5 m deep, each layer has a uniform 10 cm thickness; (2) for other lakes, the number of water layers is fixed at 50 and the layer thickness increases downward exponentially with an initial layer thickness of about 10 cm. The depth of the 1-D sediment column is set to 25 m and the sediment layer thickness also increases downward exponentially [Tan and Zhuang, 2015a]. By using a 25 m sediment column, the model can represent the permafrost portions of sediments that are very deep in yedoma landscapes and which can release a large amount of OC once thawed beneath lakes [Walter et al., 2006; Tan et al., 2015].

The overall dynamics of the carbon and phosphorus pools are governed by the following 1-D differential mass balance equations:

$$\frac{\partial[\text{DOC}]}{\partial t} = \frac{\partial}{\partial z} \left(D_w \frac{\partial[\text{DOC}]}{\partial z} \right) + f_{\text{DOC}} \times \text{LPOC} + \text{DOC}_{\text{in}} - \text{DOC}_{\text{out}} - \text{RDOC} - \text{floc}, \quad (1)$$

$$\frac{\partial[\text{DIC}]}{\partial t} = \frac{\partial}{\partial z} \left(D_w \frac{\partial[\text{DIC}]}{\partial z} \right) + f_{\text{DIC}} \times \text{LPOC} + \text{RDOC} + \text{RCH}_4 + \text{DIC}_{\text{in}} - \text{DIC}_{\text{out}} - \text{GPP}, \quad (2)$$

$$\frac{\partial[\text{POC}]}{\partial t} = V_{\text{settl}} \frac{\partial[\text{POC}]}{\partial z} + \text{GPP} + \text{POC}_s + \text{POC}_{\text{in}} - \text{POC}_{\text{out}} - \text{LPOC}, \quad (3)$$

$$\frac{\partial[\text{SRP}]}{\partial t} = \frac{\partial}{\partial z} \left(D_w \frac{\partial[\text{SRP}]}{\partial z} \right) + \lambda_{\text{DOM}} \times \text{RDOC} + \text{SRP}_{\text{in}} - \text{SRP}_{\text{out}} - \lambda_{\text{POM}} \times \text{GPP}, \quad (4)$$

where D_w is the sum of water molecular and eddy diffusivity ($\text{m}^2 \text{s}^{-1}$), V_{settl} is phytoplankton settling velocity (m s^{-1}), LPOC is metabolic loss of phytoplankton biomass ($\text{mmol C m}^{-3} \text{s}^{-1}$) including respiration, excretion and mortality, GPP is gross primary production from phytoplankton photosynthesis ($\text{mmol C m}^{-3} \text{s}^{-1}$), POC_s is the suspension of phytoplankton from sediments by bottom shear stress ($\text{mmol C m}^{-3} \text{s}^{-1}$), RDOC is DOC mineralization ($\text{mmol C m}^{-3} \text{s}^{-1}$) including microbial mineralization RDOC_b and photochemical mineralization RDOC_p , floc is the loss ($\text{mmol C m}^{-3} \text{s}^{-1}$) of DOC_{tr} due to flocculation, RCH_4 is CO₂ production from methanotrophy ($\text{mmol C m}^{-3} \text{s}^{-1}$), DOC_{in} , DIC_{in} , POC_{in} , and SRP_{in} are inflow of carbon and phosphorus ($\text{mmol m}^{-3} \text{s}^{-1}$) and DOC_{out} , DIC_{out} , POC_{out} , and SRP_{out} are outflow of carbon and phosphorus ($\text{mmol m}^{-3} \text{s}^{-1}$), f_{DOC} is exudate fraction of phytoplankton metabolic loss, f_{DIC} is respiration fraction of phytoplankton metabolic loss, and λ_{DOM} and λ_{POM} are inverses of C:P stoichiometry of dissolved organic matter (DOM) and particulate organic matter (POM), respectively. For allochthonous DOM, C:P stoichiometry is set to 199:1 [Hopkinson and Vallino, 2005]. For POM and autochthonous DOM, C:P stoichiometry is set equal to the Redfield ratio of 106:1 [Hipsey and Hamilton, 2008]. The values of the model parameters that are not subject to calibration are listed in Table 1. For two phytoplankton functional types, the model parameters are different (Table 1).

We formulate inorganic carbon fixation induced by photosynthesis as a function of sunlight, phosphorus content, and temperature [Tian, 2006; Hipsey and Hamilton, 2008; Li et al., 2010]:

$$\text{GPP} = V_m^0 f(\text{PAR}) f(T) f(\text{SRP}) \text{Chl } a, \quad (5)$$

where V_m^0 is the maximum chlorophyll-specific photosynthetic rate ($\mu\text{mol C (mg Chl)}^{-1} \text{s}^{-1}$) without nutrient and light limitation, $\text{Chl } a$ is chlorophyll a concentration (mg Chl L^{-1}), PAR is in units of $\mu\text{mol photons m}^{-2} \text{s}^{-1}$, T is water temperature ($^{\circ}\text{C}$), $f(\text{PAR})$ is the response function of photosynthesis to light

Table 1. List of New Model Parameters^a

Symbol	Definition	Small	Large	Units	Source
α	Initial slope of photosynthesis-irradiance (P-I) curve	0.0030	0.0061	$(\mu\text{mol photons})^{-1} \text{m}^2 \text{s d}^{-1}$	Li et al. [2010]
β	Photoinhibition factor	0.0017	0.0002	$(\mu\text{mol photons})^{-1} \text{m}^2 \text{s d}^{-1}$	Li et al. [2010]
$\alpha_{chl,min}$	Minimum phytoplankton C:Chl <i>a</i> ratio	30	15	g g^{-1}	Wang et al. [2009]
$\alpha_{chl,max}$	Maximum phytoplankton C:Chl <i>a</i> ratio	200	120	g g^{-1}	Wang et al. [2009]
α_{algae}	Phytoplankton density response parameter to sunlight	618	N/A	$\text{kg m}^{-3} \text{d}^{-1}$	Hipsey and Hamilton [2008]
β_{algae}	Phytoplankton density response parameter to sunlight	33	N/A	$\text{kg m}^{-3} \text{d}^{-1}$	Hipsey and Hamilton [2008]
Scsed	POC resuspension rate	0.5	0.5	$\text{mol m}^{-2} \text{d}^{-1}$	Saloranta and Andersen [2007]
f_{DIC}	Respiration fraction of phytoplankton metabolic loss	0.8	0.5	Fraction	Hanson et al. [2011]
f_{DOC}	Exudate fraction of phytoplankton metabolic loss	0.02	0.25	Fraction	Hanson et al. [2011]
T_{opt}	Phytoplankton growth optimum temperature	30	19	$^{\circ}\text{C}$	Hipsey and Hamilton [2008]
T_{std}	Phytoplankton growth standard temperature	24	17	$^{\circ}\text{C}$	Hipsey and Hamilton [2008]
T_{max}	Phytoplankton growth maximum temperature	39	22	$^{\circ}\text{C}$	Hipsey and Hamilton [2008]
θ_l	Temperature-dependence coefficient of metabolic loss	1.073	1.073	Coefficient	Hanson et al. [2011]
θ_p	Temperature-dependence coefficient of microbial mineralization	1.073	1.073	Coefficient	Hanson et al. [2011]
k_{chl}	Slope of phytoplankton C:Chl <i>a</i> ratio versus growth rate	95	70	$\text{g g}^{-1} \text{d}$	Wang et al. [2009]
k_{SRP}	Half-saturation for phosphorus uptake	0.0012	0.005	g P m^{-3}	Hanson et al. [2011]
k_{O_2}	half-saturation for DOC oxidation	1.5	1.5	$\text{g O}_2 \text{m}^{-3}$	Hanson et al. [2011]
d_A	Phytoplankton cell diameter	10^{-7}	10^{-5}	m	Hanson et al. [2011]
Symbol	Definition	Range		Units	Source
V_m^0	Maximum chlorophyll-specific photosynthetic rate	18.36–73.44		$\text{mg C (mg Chl)}^{-1} \text{d}^{-1}$	Li et al. [2010]
V_l	Maximum metabolic loss potential	0.04–0.125		Day^{-1}	Hipsey and Hamilton [2008]
$R_c^{O_2}$	Aerobic carbon degradation rate in sediment	0.00002–0.0005		Day^{-1}	Lee et al. [2012]
V_r^{aq}	Maximum DOC_{aq} biomineralization rate	0.01–0.1		Day^{-1}	Hanson et al. [2011]; Spencer et al. [2015]
V_r^{tr}	Maximum DOC_{tr} biomineralization rate	0.0005–0.05		Day^{-1}	Hanson et al. [2011]; Vachon et al. [2017]
V_m	Maximum DOC_{aq} anaerobic degradation rate	0.00001–0.0025		Day^{-1}	Lee et al. [2012]; Treat et al. [2015]
DOC_{gw}	Leached DOC concentration	7.9–93.4		g C m^{-3}	Einarsdottir et al. [2017]
r_{thaw}	Thermokarst erosion rate	0.02–1.81		m yr^{-1}	Jones et al. [2011]
Symbol	Definition	Units	Toolik Lake	Yedoma Lakes	Thermokarst Lakes
$SUVA_{305}$	Carbon-specific absorption coefficient at 305 nm	$\text{m}^3 (\text{g C})^{-1} \text{m}^{-1}$	2.9	1.7	1.8
s_g	Spectral slope of CDOM absorption	nm^{-1}	0.017	0.012	0.016
e^{-m1}	Fitted parameter related to AQY	$\text{mol C (mol photons)}^{-1}$	2.705×10^{-3}	9.017×10^{-4}	2.351×10^{-3}
$m2$	Fitted parameter related to AQY	nm^{-1}	0.017	0.012	0.016

^aInitial values are listed for parameters that are not involved in calibration. Parameter ranges are listed for parameters that are involved in sensitivity tests and calibration. The parameters given by Tan et al. [2015] are not listed.

$(f(PAR)) = \left[1 - e^{-\alpha PAR/V_m^0} \right] e^{-\beta PAR/V_m^0}$, where α is the initial slope of photosynthesis-irradiance (P-I) curve and β is the photoinhibition parameter), $f(T)$ is the response function of photosynthesis to temperature ($f(T) = \theta^T - 20 - \theta^{k_T(T-a_T)} + b_T$, where θ_p is temperature-dependence coefficient of photosynthesis, and k_T , a_T , and b_T are fitted parameters controlled by optimal temperature T_{opt} , standard temperature T_{std} , and maximum temperature T_{max} [Hipsey and Hamilton, 2008]), $f(SRP)$ is the response function of photosynthesis to phosphorus ($f(SRP) = \frac{SRP}{SRP + k_{SRP}}$, where k_{SRP} is half-saturation for phosphorus uptake). In the model, Chl *a* is simulated proportionally to phytoplankton biomass at a ratio that varies with irradiance, temperature and nutrients [Wang et al., 2009]:

$$\alpha_{chl}(z) = \alpha_{chl}^{surf} - (\alpha_{chl}^{surf} - \alpha_{chl}^{min}) \frac{\ln(PAR_{surf}) - \ln(PAR(z))}{4.605}, \quad (6)$$

$$\alpha_{chl}^{surf} = \alpha_{chl}^{max} - k_{chl} \mu_0 f(T) f(SRP), \quad (7)$$

where $\alpha_{chl}(z)$ is phytoplankton C:Chl *a* ratio at depth z , α_{chl}^{surf} is surface phytoplankton C:Chl *a* ratio, α_{chl}^{min} and α_{chl}^{max} are the minimum and maximum phytoplankton C:Chl *a* ratio, μ_0 is the maximum growth rate at 0°C , k_{chl} is the slope of phytoplankton C:Chl *a* ratio versus growth rate, and PAR_{surf} is the incoming surface PAR. Equations (6) and (7) indicate that the phytoplankton C:Chl *a* ratio changes with the PAR level in the euphotic zone where PAR is larger than 1% of the surface PAR and the surface C:Chl *a* ratio decreases linearly with the phytoplankton growth rate under nonlight limitation conditions. The respective values of μ_0 are 0.4 and 1.0 day^{-1} for small and large phytoplankton when V_m^0 is $36.72 \text{ mg C (mg Chl)}^{-1} \text{d}^{-1}$ [Li et al., 2010].

The metabolic loss of phytoplankton biomass is modeled as a function of temperature [Hanson et al., 2004]:

$$LPOC = V_l \theta_l^{T-20} [POC], \quad (8)$$

where V_l is the maximum metabolic loss potential (s^{-1}) and θ_l is temperature-dependence coefficient of metabolic loss. The biomineralization rate of DOC is modeled as a function of temperature and oxygen (O_2) level [Hipsey and Hamilton, 2008; Hanson et al., 2011]:

$$RDOC_b = V_r \theta_r^{T-20} \frac{O_2}{O_2 + k_{O_2}} [DOC], \quad (9)$$

where V_r is the maximum DOC microbial mineralization rate (s^{-1}), θ_r is temperature-dependence coefficient of microbial mineralization, and k_{O_2} is half-saturation for DOC oxidation ($mmol\ m^{-3}$). Because there could be much difference between DOC_{tr} and DOC_{aq} in recalcitrance to biomineralization [Kellerman et al., 2015], we use different V_r values for DOC_{tr} and DOC_{aq} (see Table 1). It should be noted that under low O_2 levels (less than $2.5\ mmol\ m^{-3}$), anaerobic reactions rather than aerobic reactions would dominate DOC degradation [Tang et al., 2010; Tan et al., 2015]. Anaerobic DOC degradation is modeled as a first-order reaction of labile DOC, which is determined by the maximum reaction rate (V_{nr}), temperature and O_2 suppression [Tang et al., 2010; Tan et al., 2015]. Sunlight-induced DOC degradation was rarely included in process-based lake biogeochemistry models but could be an important pathway for OC mineralization as shown in recent studies [Cory et al., 2014; Koehler et al., 2014]. Following Koehler et al. [2014], we model the photochemical degradation of DOC_{tr} as a function of irradiance spectra (varying with depth) and CDOM absorbance (varying with spectrum):

$$RDOC_p = \int_{\lambda_{min}}^{\lambda_{max}} E_{od}(\lambda, z) a_g(\lambda) \Phi(\lambda) d\lambda, \quad (10)$$

where λ_{min} and λ_{max} are the minimal and maximal wavelength (280 and 700 nm), respectively, $E_{od}(\lambda, z)$ is hourly averaged downwelling scalar irradiation at depth z ($\mu mol\ photons\ m^{-2}\ s^{-1}\ nm^{-1}$), $a_g(\lambda)$ is the CDOM absorption coefficient (m^{-1}), and $\Phi(\lambda)$ is the apparent quantum yield (AQY) of DIC photoproduction ($mol\ C\ (\mu mol\ photons)^{-1}$). The absorption coefficient $a_g(\lambda)$ is defined by the reference carbon-specific absorption coefficient at 305 nm, $SUVA_{305}$ ($m^3\ (mmol\ C)^{-1}\ m^{-1}$), as [Cory et al., 2014]:

$$a_g(\lambda) = SUVA_{305} e^{-s_g(\lambda-305)} [DOC], \quad (11)$$

where s_g is spectral slope of CDOM absorption (nm^{-1}). The AQY of DIC photoproduction is given by Koehler et al. [2014]:

$$\Phi(\lambda) = e^{-(m1+m2(\lambda-290))}, \quad (12)$$

where $m1$ and $m2$ are fitted parameters. The parameters in equations (15) and (16), i.e., $SUVA_{305}$, s_g , $m1$, and $m2$, are lake specific (see Table 1). We obtained or fitted them for yedoma, thermokarst, and glacial lakes, respectively, based on the published work [Shirokova et al., 2013; Cory et al., 2013, 2014; Manasy-pov et al., 2014; Ward and Cory, 2016]. It should be noted that the AQY parameter fitted from the work of Cory et al. [2013] would yield low DOC photolability in yedoma lakes, which is consistent with other investigations [Ward and Cory, 2016; Stubbins et al., 2017]. In contrast, tundra and thermokarst lakes, which are mainly fed by terrigenous modern-age DOC, would likely have much higher photochemical activities [Cory et al., 2014; Ward and Cory, 2016]. Unlike DOC_{tr} , DOC_{aq} is assumed to be little susceptible to sun-induced mineralization [Obernosterer and Benner, 2004]. The increase of biodegradability of terrigenous DOC after phototransformation is not included because there is still a large uncertainty in its magnitude [Obernosterer and Benner, 2004; Cory et al., 2014]. In the model, DIC production through methanotrophy is modeled as a Michaelis-Menten kinetics function of CH_4 and O_2 concentrations [Tan et al., 2015].

The phytoplankton settling velocity V_{settl} is calculated according to Stoke's law as a function of particle diameter, particle density, water density, and water viscosity [Hanson et al., 2011]. Nondiatom (i.e., cyanobacteria) can move within the water column for better light and nutrient conditions by the function of gas vesicles, a process called buoyancy control [Kromkamp and Walsby, 1990]. In the process, nondiatom makes itself float or sink to a depth for better growth through increasing or decreasing its density that is assumed to be controlled by the phytoplankton growth ratio on PAR [Hipsey and Hamilton, 2008]:

$$\Delta\rho_{algae} = (\alpha_{algae}f(PAR) - \beta_{algae})\Delta t, \quad (13)$$

where α_{algae} and β_{algae} are parameters defining phytoplankton density response to sunlight ($\text{kg m}^{-3} \text{s}^{-1}$) and Δt is time step (s). Water density is calculated as a function of water temperature and salinity [Wüest *et al.*, 1992]. Following Shirokova *et al.* [2013], we built a linear relationship between water salinity ($\mu\text{S cm}^{-1}$) and DOC (and DIC) levels based on the observational data (see supporting information Figures S11–S13). Diatom is considered to be nonmotile and has a fixed sinking speed at 0.75 m d^{-1} [Hipsey and Hamilton, 2008; Hanson *et al.*, 2011]. Because wind-induced shear stress could be strong in the water column of shallow Arctic lakes, we only activate the sinking and motion of phytoplankton in the water column when the time scale for sinking is less than the time scale for mixing [MacIntyre, 1998]. Resuspension, although relatively small, can be essential to ensure some background concentration of phytoplankton in the water column of Arctic lakes after a long ice-covered winter season [Saloranta and Andersen, 2007]. This source term POC_s is modeled as a function of area-specific resuspension rate $Scsed$ but subjects to the limitation of phytoplankton stock on surface sediments [Saloranta and Andersen, 2007]. Different from Hipsey and Hamilton [2008], we do not include the degradation of phytoplankton detritus in the water column during settling because the settling time could be very short in usually shallow Arctic lakes.

The load of allochthonous carbon consists of loadings from precipitation, litterfall, surface runoff, and leaching [Hanson *et al.*, 2004]. According to Hanson *et al.* [2014], the load of OC from precipitation is the product of precipitation (mm) and a constant precipitation DOC concentration (2 mg C mm^{-1}), and the load of OC from litterfall is the product of lake shoreline in canopy (m) and the annual mean litterfall rate ($1 \text{ g C m}^{-1} \text{ d}^{-1}$). It should be noted that Hanson *et al.* [2014] used these typical values for temperate lakes where terrestrial ecosystems are usually much more productive than those surrounding Arctic lakes. Thus, the contribution of precipitation and litterfall to the carbon dynamics of the study lakes could be overestimated by our model. Many studies indicated that the lake catchment makes a major contribution to inland water DOC through leaching and the wetland fraction in the lake catchment is a major control for this loading [Evans *et al.*, 2005; Roulet and Moore, 2006; Monteith *et al.*, 2007; Einarsdottir *et al.*, 2017]. In the ALBM, the leached DOC is calculated as a function of subsurface DOC discharge (the product of subsurface discharge and DOC concentration) and the catchment wetland fraction [Hanson *et al.*, 2004]. For simplification, we assume that the seasonal variability of DOC leaching is solely driven by the seasonal variability of subsurface discharge. This means that the subsurface DOC concentration for each lake is fixed at a level specified by a free parameter DOC_{gw} . Meanwhile, the leached DIC is assumed to be 25% of the leached DOC and the POC load through leaching is not included [Molot and Dillon, 1996]. For lakes with inlet streams, the load of DOC, DIC, POC, and SRP through surface discharge could also be substantial [Einarsdottir *et al.*, 2017]. The amounts can be determined by water discharge and substance concentrations. Similarly, the loss of carbon and phosphorus through surface water outflow can be estimated by surface water outflow and dissolved substance concentrations.

Recent studies indicated that there could be a large amount of labile OC entering thermokarst lakes (both yedoma and nonyedoma) from their active thermokarst margins [Walter *et al.*, 2006; Laurion *et al.*, 2010; Walter Anthony *et al.*, 2014; Manasyov *et al.*, 2015]. To realistically simulate the carbon dynamics in yedoma and nonyedoma thermokarst lakes, this important carbon source must be included. In our model, the carbon load from thermokarst erosion is estimated as a product of the length of eroded lake shores, the thermokarst erosion rate (r_{thaw}), and soil carbon density (kg C m^{-3}). The above carbon load does not include any OC mobilized from thawing permafrost beneath yedoma and nonyedoma thermokarst lakes (taliks), which as described in Tan *et al.* [2015] is incorporated into the ^{14}C -depleted carbon pool of sediments and can be oxidized through either aerobic or anaerobic mineralization. For yedoma lakes, due to their anoxic hypolimnion [Walter Anthony *et al.*, 2014; Martinez-Cruz *et al.*, 2015], usually only anaerobic oxidation occurs in sediments. CO_2 , CH_4 , and P that are produced from OC oxidation in sediments can enter water columns through ebullition (CO_2 and CH_4 only) or diffusion. We assume that 50% of the DOC load from thermokarst erosion consists of the low-molecular-weight organic acids acetate and butyrate [Spencer *et al.*, 2015; Drake *et al.*, 2015] that are less colorful and can be rapidly used by microbes. The carbon density of yedoma permafrost with ice wedge included is set to 29.3 kg C m^{-3} [Schirmer *et al.*, 2011].

For northern high-latitude lakes, von Wachenfeldt and Tranvik [2008] observed that terrigenous DOM can be removed from the water column via flocculation at a rate approximately equal to mineralization. In the

model, the flocculation of DOC (*floc*) is calculated during open-water seasons as a function of the DOC_{tr} level with $[DOC_{tr}] \times 0.0019 \text{ day}^{-1}$ [von Wachenfeldt and Tranvik, 2008]. In winter, both allochthonous and autochthonous DOM are removed through chemical coagulation when trapped in ice layers [Manasypov et al., 2015].

It should be noted that although this carbon model refers to the CAEDYM model [Hipsey and Hamilton, 2008] for simulating microbial degradation, the settling velocity of inorganic particles, and the growth, movement and mortality of phytoplankton, the two models are much different in regard to design and applications. The ALBM can simulate several physical and biogeochemical processes that are important for understanding the carbon dynamics in Arctic lakes but are lacking in the CAEDYM and its coupled hydrodynamics models (e.g., the DYRESM model), for example, the dynamics of ice and snow layers, the freezing and thawing of lake sediments, the photomineralization and flocculation of DOC, and the production, transport and oxidation of CH_4 [Cory et al., 2014; Manasypov et al., 2015; Sepulveda-Jauregui et al., 2015]. In addition, the ALBM explicitly simulates the change of carbon to chlorophyll ratios in phytoplankton species with water depth and light instead of specifying a fixed number as is done in the CAEDYM model. But we acknowledge that there are some biogeochemical processes implemented in CAEDYM but not ALBM, which are found to be important in understanding the carbon dynamics of lakes. For example, the CAEDYM model can simulate more phytoplankton groups (e.g., dinoflagellates and chlorophytes) and aquatic organisms at higher trophic levels (e.g., zooplankton and jellyfish) [Hipsey and Hamilton, 2008]. The CAEDYM model can also simulate the change of internal nutrient stoichiometry and the limitation of phytoplankton growth by nitrogen and silica [Hipsey and Hamilton, 2008]. Future studies will be needed to explore the influences of these processes on the carbon dynamics of Arctic lakes.

2.1.2. Solar Radiation Transfer Model

To simulate the spectral distribution of solar radiation for photosynthesis and photochemistry modeling, we integrate the Simple Model of the Atmospheric Radiative Transfer of Sunshine (SMARTS) developed by Gueymard [1995] into the ALBM. The SMARTS model can predict the direct beam, diffuse, and global clear-sky irradiance incident on surfaces of any geometry at the Earth's surface and cover the whole shortwave solar spectrum of 280–4000 nm [Gueymard, 2005]. The SMARTS model is superior to most other radiation transport models in that it can simulate high-resolution solar spectral distribution efficiently and robustly [Gueymard, 1995, 2005].

The simulated clear-sky solar radiation from the SMARTS model needs to be adjusted to account for the effects of clouds. We assume that solar radiation is attenuated by clouds equally along the entire spectrum [Koehler et al., 2014] and the reduced fraction τ is given by Kasten and Czeplak [1980]:

$$\tau = (1 - \tau_{\text{overcast}})(cc/8)^\alpha, \quad (14)$$

where cc is total cloud cover in Octa (0–8), and $\tau_{\text{overcast}} = 0.37$ and $\alpha = 2.1$ are fitted parameters [Koehler et al., 2014]. The variable cc can be converted from cloudiness in fraction by using a conversion table in Boers et al. [2010]. The presence of clouds also increases the diffuse fraction of irradiance by spectrum-dependent ratios. To be simple, we use a broadband correction function introduced by Grant and Gao [2003] for the correction of ultraviolet radiation (UV) in the temperate regions to account for this increase:

$$\Delta D_\lambda = a_\lambda + b_\lambda e^{-0.5 \times \left(\left[\frac{cc - c_\lambda}{d_\lambda} \right]^2 + \left[\frac{\theta - e_\lambda}{f_\lambda} \right]^2 \right)}, \quad (15)$$

where ΔD_λ is diffuse fraction increment due to cloud cover, θ is solar zenith angle in decimal degree, and a_λ , b_λ , c_λ , d_λ , e_λ , and f_λ are fitted parameters. For ultraviolet-B radiation (UVB), $a_\lambda = -0.009$, $b_\lambda = 3.73$, $c_\lambda = 28$, $d_\lambda = 9.4$, $e_\lambda = 26$, and $f_\lambda = 26$ [Grant and Gao, 2003]. For other radiation bands, i.e., ultraviolet-A radiation (UVA), photosynthetically active radiation (PAR) and near-infrared radiation (IR), $a_\lambda = -0.031$, $b_\lambda = 1.30$, $c_\lambda = 17$, $d_\lambda = 6.3$, $e_\lambda = 28$, and $f_\lambda = 30$ [Grant and Gao, 2003]. On days of overcast sky, the diffuse fraction of all radiation bands is fixed at 0.95 [Grant and Gao, 2003]. As validated in the supporting information Figures S1–S6, the method of Grant and Gao [2003] can be extended to the pan-Arctic regions and used for the PAR and IR bands. After the cloud correction, we further constrain the simulated total solar radiation using the remotely sensed $1^\circ \times 1^\circ$ SYN1deg radiation product of NASA Clouds and Earth's Radiant Energy System (CERES; http://ceres.larc.nasa.gov/order_data.php).

The transmittance of the above water surface irradiance through the water-air interface is calculated separately for the diffuse and direct radiation following the method of *Koehler et al.* [2014]. The transmittance of diffuse radiation is fixed at 0.934 [*Koehler et al.*, 2014]. The transmittance of direct radiation, T_d , is defined by Fresnel's law [*Kirk*, 2011]:

$$T_d = 1 - \frac{1}{2} \left(\frac{\sin^2(\theta - \theta_w)}{\sin^2(\theta + \theta_w)} + \frac{\tan^2(\theta - \theta_w)}{\tan^2(\theta + \theta_w)} \right), \quad (16)$$

where θ_w is the refracted solar zenith angle, calculated as $\sin^{-1}(\sin \theta / 1.33)$. To calculate the available irradiance for photosynthesis and photomineralization, the underwater irradiance spectra are converted to scalar irradiance using a modified empirical relationship between the average cosine of the downwelling irradiance μ_d (inverse of the scalar), the diffuse fraction f_{diff} and the refracted solar zenith angle [*Fichot and Miller*, 2010]:

$$\frac{1}{\mu_d} = \frac{1 - f_{diff}}{\cos \theta_w} + \frac{f_{diff}}{0.859}. \quad (17)$$

The attenuation of irradiance by snow and ice during ice cover seasons has been given by *Tan et al.* [2015]. Below the water surface, light can be absorbed by water and chromophoric dissolved organic matter (CDOM), used by phytoplankton and backscattered by organism detritus. We model the light attenuation based on the light absorption spectrum and substance abundance of water, CDOM and chlorophyll a , respectively, as described by *Kirk* [2011].

2.1.3. Revised Model Components

Due to the incorporation of phytoplankton metabolism and DOC mineralization, the governing equation for dissolved O_2 in *Tan et al.* [2015] is modified as

$$\frac{\partial [O_2]}{\partial t} = \frac{\partial}{\partial z} \left(D_w \frac{\partial [O_2]}{\partial z} \right) + \alpha_{O_2} \times GPP - RDOC - f_{DIC} \times LPOC - 2 \times RCH_4, \quad (18)$$

where α_{O_2} is the photosynthetic quotient (the ratio of O_2 production to CO_2 fixation). The quotient is set to 1.1 in the model [*Kirk*, 2011; *Cory et al.*, 2014]. The methanotrophic consumption of O_2 , RCH_4 , is defined as a Michaelis-Menten function of CH_4 and O_2 concentrations [*Martinez-Cruz et al.*, 2015; *Tan et al.*, 2015].

One benefit of integrating the solar radiation transfer model is the better representation of light extinction coefficients in different lakes during different seasons. In *Tan et al.* [2015], the light extinction coefficient of Arctic lakes was parameterized as an empirical function of lake depth and a trophic state factor that reflects a negative correlation between lake trophic status and depth [*Subin et al.*, 2012]. The trophic state factor was added as a light extinction coefficient correction for yedoma lakes in the bLake4Me model because yedoma lakes can be more trophic than other Arctic lakes even when their depths are similar [*Walter Anthony et al.*, 2014; *Sepulveda-Jauregui et al.*, 2015]. However, since lake trophic state can also be affected by other factors (e.g., lake area, temperature, and catchment characteristics), this expression is inaccurate. In ALBM, light extinction coefficient is instead determined by water depth, CDOM concentration, chlorophyll a concentration and detritus concentration that vary among lakes and with boundary conditions.

Recently, several studies demonstrated that the wind-based models as used in the bLake4Me model [*Tan et al.*, 2015] are likely to underestimate air-water gas transfer velocity (piston velocity) during surface cooling [*MacIntyre et al.*, 2010; *Heiskanen et al.*, 2014]. To correct this bias, several alternative approaches (e.g., the surface renewal model) were proposed to incorporate the effects of both wind speed and buoyancy flux [*Heiskanen et al.*, 2014]. In ALBM, following these studies, we instead formulate piston velocity k_{SR} ($m s^{-1}$) using the surface renewal model [*Heiskanen et al.*, 2014]:

$$k_{SR} = \sqrt{(0.00015U)^2 + (0.07(-\beta z_{AML})^{\frac{1}{3}})^2} Sc^{-0.5}, \quad (19)$$

where U is wind speed at 2.0 m ($m s^{-1}$), β is buoyant flux ($\beta < 0$ if losing heat and vice versa), z_{AML} is the depth of the actively mixing layer (m), and Sc is Schmidt number. Another change we have made to the lake model is to calculate convective mixing in the water column (e.g., spring/fall turnover) by balancing the total available kinetic energy and the mixing potential energy, as described in the MyLake model [*Saloranta and Andersen*, 2007].

Overall, the ALBM uses the same methods as the bLake4Me model in simulating heat transfer in the water and sediment columns, the dynamics of ice and snow layers, permafrost thawing beneath yedoma and nonyedoma thermokarst lakes, and CH₄ production, oxidation, and transport. However, the ALBM can simulate DOC biomineralization and photomineralization, DOC flocculation, and phytoplankton metabolism, which are not represented in the bLake4Me model. In addition, the ALBM uses better methods to simulate solar radiation transfer, gas piston velocity, and lake convective mixing. Importantly, by this upgrade, the ALBM can simulate the dynamics of both CO₂ and CH₄ in the water and sediment columns of Arctic lakes.

2.2. Model Evaluation

2.2.1. Data Collection

To evaluate the integrated solar radiation transfer model, we collected ground solar radiation measurements from the Baseline Surface Radiation Network (BSRN) stations [Ohmura *et al.*, 1998] (<http://www.bsrn.awi.de/>). In BSRN, the components of solar radiation (total, direct normal, and diffuse) are continuously measured at these sites at 1–3 min intervals for the radiation bands of UVA, UVB, PAR, and IR. The BSRN network currently operates 48 stations that cover the latitude range from 90°S to 80°N. Within them, we chose two northern high-latitude stations (BAR and TOR) where data are available during the period of 2001–2010 and the impacts of topography and vegetation on solar radiation are minimal. The BAR station is located in a flat coastal tundra region of Barrow, Alaska, USA (71.323°N/156.607°W) and records global and diffuse solar radiation (basic measurements) at the 1 min interval [Dutton, 2007]. The TOR station is located in a flat grassland region of Toravere, Estonia (58.254°N/26.462°E) and also records basic measurements at the 1 min interval [Kallis, 2007]. Only measurements from days with more than 90% valid observed values are used for comparison. Following Grant and Gao [2003], we retrieved the air forcing data (e.g., cloud cover classification) for each BSRN station from the Automated Surface Observation System (<http://www1.nccdc.noaa.gov/pub/data/noaa/>). For comparison, we also downscaled the CERES remotely sensed direct and diffuse PAR and UV radiations to the BAR and TOR sites [Trenberth *et al.*, 2009]. The total ozone column was retrieved from the 0.5° × 0.5° monthly Multi Sensor Reanalysis (MSR) data version 2 of Tropospheric Emission Monitoring Internet Service [van der A *et al.*, 2010]. The aerosol optical depth (AOD) at 550 nm was retrieved from the 0.5° × 0.5° SeaWiFS Deep Blue Level 3 Long-term Aerosol Data Monthly Products Version 4 [Sayer *et al.*, 2012]. For areas where the SeaWiFS data set does not cover, we used the AOD monthly values from the global Max-Planck-Institute Aerosol Climatology version 2 (MAC-v2) [Kinne *et al.*, 2013]. The validation of the solar radiation transfer model at the two stations is shown in supporting information Figures S1–S6. Clearly, the model performs well in simulating the broadband solar radiation at the BAR and TOR station. Additionally, the simulated fine-scale spectrum of solar radiation is also highly consistent with what Cory *et al.* [2014] measured above the water surface of Toolik Lake on 29 June 2012 (results not shown).

The data to evaluate the carbon cycle model were collected from three yedoma lakes (Shuchi Lake: 68.746°N/161.393°E, Tube Dispenser Lake: 68.756°N/161.388°E, and Grass Lake: 68.749°N/161.414°E) on the East Siberian coastal plain, two thermokarst lakes within a permafrost peatland complex from an experimental site near Seida (67.05°N/62.93°E, 100 m asl) in the subarctic tundra of the Komi Republic, Russia, and one glacial kettle lake (Toolik Lake: 68.63°N/149.6°W) on the North Slope of Alaska, as listed in Table 2. These small Arctic lakes are selected because recent studies showed that small lakes and ponds could have

Table 2. Characteristics of the Study Lakes

Site Name	Location	Max Depth (m)	Area (ha)	Catchment (ha)	Classification ^a	Source ^b
Shuchi Lake	69°N/161°E	11.0	5.8	31.7	C1	UAF
Tube Dispenser Lake	69°N/161°E	17.0	11.0	81.5	C1	UAF
Grass Lake	69°N/161°E	12.0	0.5	16.9	C2	UAF
Seida Lake A	67°N/63°E	2.6	0.9	15	C3	UEF
Seida Lake B	67°N/63°E	2.2	3.0	51	C4	UEF
Toolik Lake	68.4°N/149.4°W	25.0	149.0	66,900	C5	LTER

^aC1, tundra/taiga tree line, continuous permafrost, yedoma with active thermokarst expansion; C2, tundra/taiga tree line, continuous permafrost, yedoma without active thermokarst expansion; C3, tundra, discontinuous permafrost, nonyedoma with intermediate peat walls and thermokarst erosion; C4, tundra, discontinuous permafrost, nonyedoma with high peat walls and ongoing thermokarst erosion; C5, kettle lake formed in continuous permafrost, nonthermokarst lake. C1–C4 are thermokarst lakes.

^bUAF, Water and Environmental Research Center at University of Alaska, Fairbanks [Walter Anthony *et al.*, 2014]; UEF, University of East Finland, Kuopio [Marushchak *et al.*, 2013]; LTER, Arctic Long Term Ecological Research Site (<http://ecosystems.mbl.edu/ARC/lakes/lakesdata.html>).

particularly large contribution to inland water CO₂ and CH₄ fluxes and may be more vulnerable to climate change [Holgerson and Raymond, 2016]. The collected data for model evaluation include (1) discrete daily measurements of dissolved CO₂ at the surface water of the Seida lakes during 2007–2008, (2) discrete biweekly measurements of dissolved CO₂, DOC, and O₂ at different depths of the three yedoma lakes during 2003, and (3) discrete daily measurements of chlorophyll *a*, phytoplankton productivity, dissolved O₂, and water temperature at different depths of Toolik Lake during 2014, which were measured by the research team at the Arctic Long Term Ecological Research Site (LTER) and maintained by Arctic LTER Lakes Data Portal [Giblin *et al.*, 2005; Giblin, 2006; Giblin *et al.*, 2010] (<http://arc-lter.ecosystems.mbl.edu/lakes-data>). Diffusive CO₂ fluxes were measured at each lake in the summer time of the study years. The diffusive CO₂ fluxes of Toolik Lake were estimated using the eddy covariance method of Eugster *et al.* [2003] that includes both wind and convective mixing as mechanisms. For the three yedoma lakes, the diffusive CO₂ fluxes were estimated by applying Fick's law to the measurements of dissolved CO₂ in surface water (supporting information Figure S14) following the boundary layer method of Kling *et al.* [1992]. For the two Seida lakes, the diffusive CO₂ fluxes were estimated from load wind speed and surface water dissolved CO₂ [Marushchak *et al.*, 2013] using the thin boundary layer model following Repo *et al.* [2007]. It should be noted that these three methods are not always consistent in predicting the temporal variability of CO₂ outgassing. For example, the eddy covariance method tends to show higher diel variations of CO₂ fluxes at Toolik Lake during summer [Eugster *et al.*, 2003]. Clearly, this discrepancy might introduce additional systematic uncertainty to model evaluation.

The daily boundary and hydrological conditions to drive the model on the study lakes are shown in supporting information Figures S7–S10. As boundary conditions were not measured for the yedoma lake site, we extracted them following Tan *et al.* [2015] from a 0.75° × 0.75° resolution data set of European Center for Medium-Range Weather Forecasts (ECMWF) Interim re-analysis (ERA-Interim) [Dee and Uppala, 2009] (http://apps.ecmwf.int/datasets/data/interim_full_daily/). For the Seida site, the boundary conditions were measured at the nearby Vorkuta station, Komi Republican Center for Hydrometeorological and Environmental Monitoring. For Toolik Lake, the boundary conditions and the discharge and chemistry of inlet and outlet streams were measured by Toolik Field Station [Environmental Data Center Team, 2016] and Arctic LTER [Kling, 2005, 2010] (<http://arc-lter.ecosystems.mbl.edu/lakes-data>). The water flow of the study lakes excluding stream discharge was calculated from a 0.25° resolution global data set of land hydrology simulated by the Variable Infiltration Capacity (VIC) Macroscale Hydrologic Model [Sheffield and Wood, 2007], as described in supporting information Text S1 [Kling *et al.*, 2000; Schwanghart and Kuhn, 2010; Paytan *et al.*, 2015]. It should be noted that because the total water flow is used for the Seida and yedoma lakes (supporting information Text S1), the parameter DOC_{gw} in fact represents the average DOC concentration in the surface and subsurface water flow for these lakes. The proportion of lake shore with canopy was extracted from a 30 arc sec resolution global data set of percent tree cover [DeFries *et al.*, 2000] (<http://glcf.umd.edu/data/tree-cover/>). Other data sets used in this study (e.g., SOC) are from Tan *et al.* [2015].

2.2.2. Model Sensitivity Analysis and Calibration

We analyzed the sensitivity of net primary production (NPP), biomineralization, and photomineralization simulations at Shuchi Lake to 22 uncertain parameters, in which 14 parameters have been described in Tan *et al.* [2015, Table 2] and 8 new parameters are presented in Table 1. In contrast to Tan *et al.* [2015], this sensitivity analysis was conducted through a two-step process to reduce the uncertainty and computation cost of the variance-based Sobol's sensitivity index analysis. In the first step, we implemented a screening test over the total 22 parameters to identify the most influential ones. The theoretical basis for the low computation cost screening test is the Pareto principle that 80% of the variation in model outputs is contributed by 20% of all parameters [Saltelli *et al.*, 2000]. In the second step, we performed a quantitative, explicit evaluation of the importance and interactions among the selected five parameters as described in Tan *et al.* [2015].

The screening test was implemented based on the Morris elementary effects method for global sensitivity analysis that perturbs only one input parameter in each model run [Morris, 1991]. For each sensitivity test of certain model output, 160 uniformly perturbed parameter samples were selected from a sample candidate pool with 1600 repetitions of experiment design via space-filling improvement [Campolongo *et al.*, 2007] and a total of $160 \times (22 + 1) = 3680$ model runs were conducted. The importance of each parameter was measured by the mean of the absolute values of the parameter's elementary effect that is the ratio of model

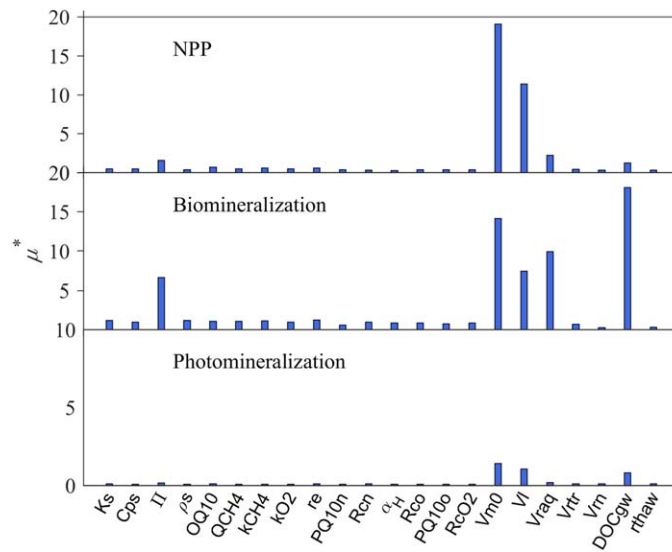


Figure 2. Screening test results (μ^* : the ratio of model output variation to parameter variation) for NPP, biomineralization, and photomineralization. K_s , thermal conductivity of solid particles in sediments; C_{ps} , heat capacity of solid particles in sediments; Π , sediments porosity; ρ_s , density of solid particles in sediments; Q_{10} , CH_4 oxidation Q_{10} ; Q_{CH_4} , CH_4 oxidation potential; k_{CH_4} , half-saturated CH_4 coefficient of CH_4 oxidation; k_{O_2} , half-saturated O_2 coefficient of CH_4 oxidation; r_e , ebullition rate; $P_{\text{Q}_{10}}^0$, CH_4 production Q_{10} of ^{14}C -enriched carbon pool; R_c^0 , decomposition fraction of ^{14}C -enriched carbon pool; α_H , vertical dampening factor of ^{14}C -enriched carbon pool; R_c^0 , decomposition fraction of ^{14}C -depleted carbon pool; $P_{\text{Q}_{10}}^0$, CH_4 production Q_{10} of ^{14}C -depleted carbon pool; R_c^0 , fraction of aerobic carbon degradation; V_m^0 , chl a -specific light saturated growth rate; V_b , metabolic loss rate; V_r^{aq} , aquatic DOC microbial degradation rate; V_r^{tr} , terrestrial DOC microbial degradation rate; V_m , anaerobic DOC degradation rate; DOC_{gw} , subsurface DOC concentration; and r_{thaw} , thermokarst erosion rate.

Lake, the parameters were calibrated using the observed eddy covariance net CO_2 fluxes, chlorophyll a , and dissolved O_2 . For the three yedoma lakes, the optimum parameters were searched by minimizing the difference between the observed and modeled CO_2 fluxes, dissolved O_2 , DOC, and DIC at Shuchi Lake. For the two thermokarst lakes, the parameters were calibrated using the observed CO_2 fluxes at Seida A Lake.

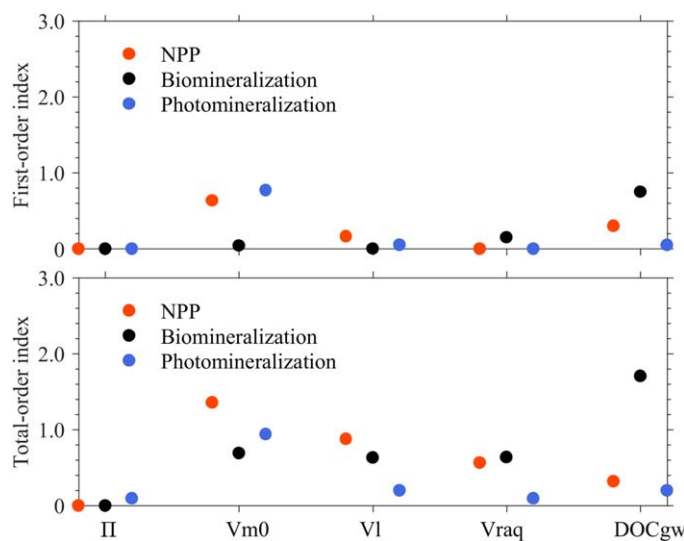


Figure 3. Sobol's estimates of first-order and total-order sensitivity indices of NPP, biomineralization, and photomineralization simulations to the five key parameters identified in Figure 2.

output variation to parameter variation (μ^*) [Campolongo *et al.*, 2007]. Five out of 22 parameters with the highest μ^* were selected for the Sobol's sensitivity test.

The Sobol's sensitivity test produces two indices: (1) the first-order sensitivity index represents the first-order contribution of a specific parameter to the output variance and (2) the total-order sensitivity index represents both the first-order and higher-order contribution (including parameter interaction) of a specific parameter to the output variance [Sobol, 1993; Saltelli *et al.*, 2010].

We calibrated the ALBM using a Monte-Carlo-based Bayesian recursive parameter estimation method separately for each lake type [Tang and Zhuang, 2009; Tan and Zhuang, 2015a, 2015b]. Since the modeled lake temperature and CH_4 dynamics have been evaluated in details by Tan *et al.* [2015], the related processes and parameters are not evaluated again in this study. For Toolik

3. Results and Discussion

3.1. Parameter Sensitivity Analysis

Through the screening test, we identified chlorophyll-specific photosynthetic potential (V_m^0), metabolic loss potential (V_b), aquatic DOC biomineralization potential (V_r^{aq}), subsurface DOC concentration (DOC_{gw}), and sediment porosity (Π) as the most influential parameters in simulating NPP, biomineralization, and photomineralization (Figure 2). For these five parameters, their individual sensitivity indices in the Sobol's test are presented in Figure 3. It is not surprising that the net productivity of Shuchi Lake is sensitive to V_m^0 and V_b because large V_m^0 means high

fixation rates of inorganic carbon by photosynthesis and large V_I means high loss rates of phytoplankton biomass by autotrophic respiration. In contrast, DOC biomineralization is most sensitive to the DOC load from land and the mineralization rate, consistent with the claim that the release of labile carbon from thawing yedoma permafrost sustains high CO_2 fluxes [Sepulveda-Jauregui *et al.*, 2015]. Biomineralization is also sensitive to V_m^0 and V_I because the exudate of phytoplankton biomass is a labile OC source for microbes. The growth of phytoplankton can reduce photomineralization through the shading effect; thus photomineralization is sensitive to V_m^0 . The significance of Π to the simulations can be explained by the impacts of Π on the conductivity of carbon and nutrients in sediments and at the water-sediment interface. When comparing the five key parameters, we find that DOC_{gw} may be more influential than other parameters in determining CO_2 fluxes from yedoma lakes.

3.2. Site-Level Model Experiments

Because many processes have been incorporated into the ALBM, it can be used for different purposes. As our focus is to understand the contribution of Arctic lakes to the global carbon cycle, to reproduce the observed CO_2 fluxes from the study lakes is our top priority. Additionally, it is also important to understand the key carbon processes controlling CO_2 fluxes in the site-level model evaluation.

3.2.1. Alaskan Glacial Lake

The ALBM can generally reproduce the temporal variability of CO_2 fluxes from an Alaskan glacial lake, Toolik Lake, during the ice-free period from 29 June to 20 August 2014 covered by continuous flux measurements (Figure 4). During the period, the modeled and observed mean daily CO_2 fluxes are 0.14 and 0.15 ± 0.07 $\text{g C m}^{-2} \text{d}^{-1}$, respectively. Regarding the carbon processes, the model well reproduces phytoplankton primary production (Figure 4). According to Crump *et al.* [2003], annual primary production in Toolik Lake was about 12 $\text{g C m}^{-2} \text{yr}^{-1}$ in 1996 and 2000, insignificantly different from our estimate of 12.38 $\text{g C m}^{-2} \text{yr}^{-1}$ (see section 3.3). The consistency of the modeled and observed primary production can also be supported by the model's good performance on chlorophyll *a* simulations (Figure 4). During the study period, there were two chlorophyll *a* peaks: one was onset with the occurrence of turnover in spring and another was onset with the occurrence of turnover in fall (Figures 4 and 5). These mixing events brought nutrients from deep water to surface water [Kling *et al.*, 1992; MacIntyre *et al.*, 1999] and drove algae growth. During the calm

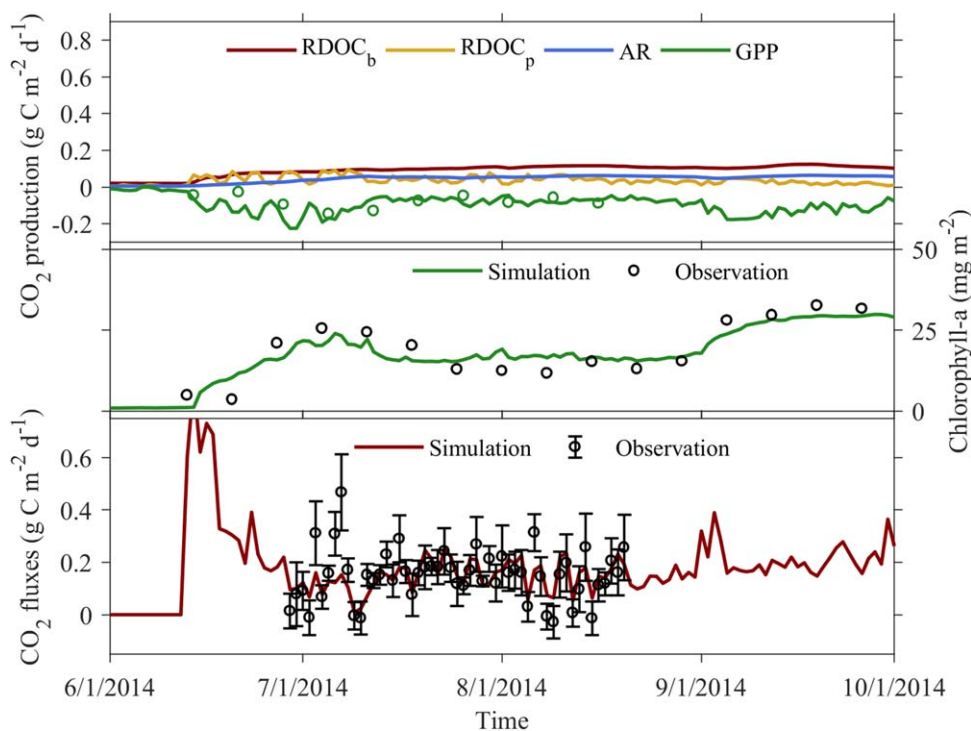


Figure 4. Dynamics of CO_2 production and fixation, chlorophyll *a*, and CO_2 fluxes at Toolik Lake from June to September 2014. Symbols represent the observed values (the observed CO_2 fluxes are aggregated to daily means \pm standard deviation) and lines represent the simulated daily mean values.

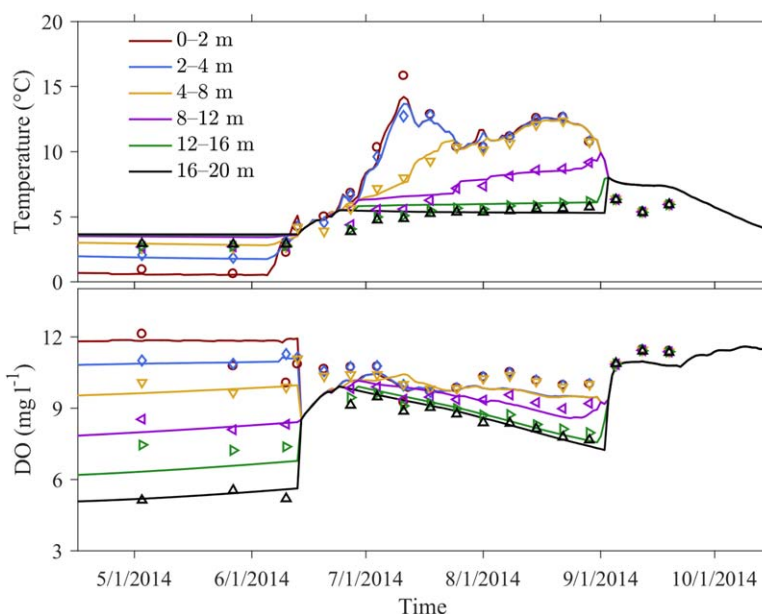


Figure 5. Dynamics of water temperature and dissolved O₂ (DO) at different depths of Shuchi Lake from April to October 2014. Symbols represent the observed values and lines represent the simulated values.

period of the open-water season, algae growth declined due to nutrient limitation [Lewis, 2011] even though solar radiation was still strong (Figure 4). The timing of the two peaks and the seasonal minimum is excellently represented by the model, but the seasonal amplitude is smaller than that in the observations possibly due to the underestimate of biomass to chlorophyll *a* ratios in the model. We do not have daily observations to evaluate microbial and photochemical mineralization directly. But during the ice-free seasons of 2011–2013, Cory *et al.* [2014] reported that the mean biomineralization and photomineralization rates were 0.08 ± 0.02 and 0.05 ± 0.01 g C m⁻² d⁻¹, respectively. These reported values are close to the simulated biomineralization and photomineralization rates (0.10 g C m⁻² d⁻¹ and 0.04 g C m⁻² yr⁻¹, respectively) during the ice-free period of 2014. The biomineralization simulation can be further supported by the consistency of the simulated and observed dissolved O₂ in the deep water of Toolik Lake (Figure 5). Although deep water O₂ was recharged in spring and fall during turnover (Figure 5), it was mainly governed by microbial mineralization when convective mixing was weak in summer.

There are some discrepancies between the simulated and observed daily CO₂ fluxes (Figure 4). The modeled CO₂ fluxes show less day-to-day variability than the observations. The less variable CO₂ fluxes could have two causes: (1) because the model is driven by daily boundary conditions, nocturnal water mixing and the corresponding variable CO₂ fluxes [Podgrajsek *et al.*, 2015] are not well simulated and (2) the day-to-day variability of the observed CO₂ fluxes was driven by the variations of carbon loading through water flow which are not well resolved by the driving hydrological and chemical conditions, especially the subsurface flow. The modeled CO₂ fluxes are also lower than the observations in early July. Since the discrepancy occurred when high DIC concentrations were measured in stream discharge (supporting information Figure S8), it is possible that the observed high fluxes were caused by the large external DIC inputs at the littoral zone of Toolik Lake where the stream and subsurface DIC is less diluted. In addition, by using a 1-D lake model to simulate an over 1 km² 3-D lake (such as Toolik Lake), the model needs to assume horizontal homogeneity within each layer. This assumption causes the model unable to accurately represent the increased dynamics during shifting wind directions and changing wind speeds that increases the upwelling of CO₂ [Eugster *et al.*, 2003]. In the experiment, we simulated high CO₂ fluxes during the turnover in spring and fall when measurements were not available. It should be noted that the similar high CO₂ fluxes during turnover have been reported for other lakes [Aberg *et al.*, 2010].

3.2.2. Siberian Yedoma Lakes

In all the yedoma lakes, the temporal variability of the modeled and observed CO₂ fluxes are consistent during the open-ice season of 2003: there were moderate CO₂ fluxes in later spring after ice was off, low CO₂

fluxes in summer and high CO₂ fluxes in fall before ice onset (Figures 6–8). By comparing the temporal variability of CO₂ fluxes with the dynamics of water stratification [Tan et al., 2015, Figures 2 and 5] and deep water DIC and DOC (Figures 6–8), it is clear that the seasonality of CO₂ fluxes during 2003 was mainly driven by CO₂ accumulation in deep water through DOC degradation and CH₄ oxidation and CO₂ upwelling during water mixing. And as suggested by previous studies [Walter et al., 2006; Walter Anthony et al., 2014], it is likely that the leached labile OC from thawing yedoma permafrost was rapidly mineralized in the water and sediment columns, sustaining high CO₂ accumulation in the yedoma lakes. Due to high DOC and DIC concentrations, the salinity of the deep water in the yedoma lakes is large (supporting information Figure S12). Thus, the yedoma lakes became stratified only a few days after ice was off because of the rising solar radiation and air temperature. Correspondingly, the strong CO₂ fluxes in spring observed at Toolik Lake are not simulated at the yedoma lakes. The modeled mean daily CO₂ fluxes during the open-water period of 2003 at Shuchi Lake, Tube Dispenser Lake and Grass Lake are 0.26, 0.22, and 1.24 g C m⁻² d⁻¹, respectively. These values are close to the observed mean daily CO₂ fluxes (0.29 g C m⁻² d⁻¹ for Shuchi Lake, 0.21 g C m⁻² d⁻¹ for Tube Dispenser Lake, and 1.62 g C m⁻² d⁻¹ for Grass Lake). The simulated high CO₂ fluxes from Grass Lake are mainly stimulated by the strong biomineralization in sediments which induces the upward carbon flux of 1.40 g C m⁻² d⁻¹ at the water-sediment interface during the open-water period.

During the open-water period, due to strong stratification and heterotrophic respiration, the hypolimnetic water of the yedoma lakes was largely anoxic and the epilimnetic O₂ was only restored during a few days around ice breakup when surface reaeration was stronger than respiration (Figures 6–8). The anoxic waters and sediments of the yedoma lakes provide favorable conditions for methanogenesis, which was documented by many studies [Walter et al., 2006; Greene et al., 2014; Martinez-Cruz et al., 2015; Sepulveda-Jauregui et al., 2015; Tan et al., 2015]. Because spring mixing was weak and nutrients gradually increased as the thermocline deepened [Walter Anthony et al., 2014; Sepulveda-Jauregui et al., 2015], chlorophyll *a* increased steadily in the summer. It maintained at high levels during strong fall mixing even though solar radiation declined largely. Here we do not have observed phytoplankton primary production or chlorophyll *a* to support the above simulations. Because dissolved O₂ is balanced by O₂ gains (through primary production and

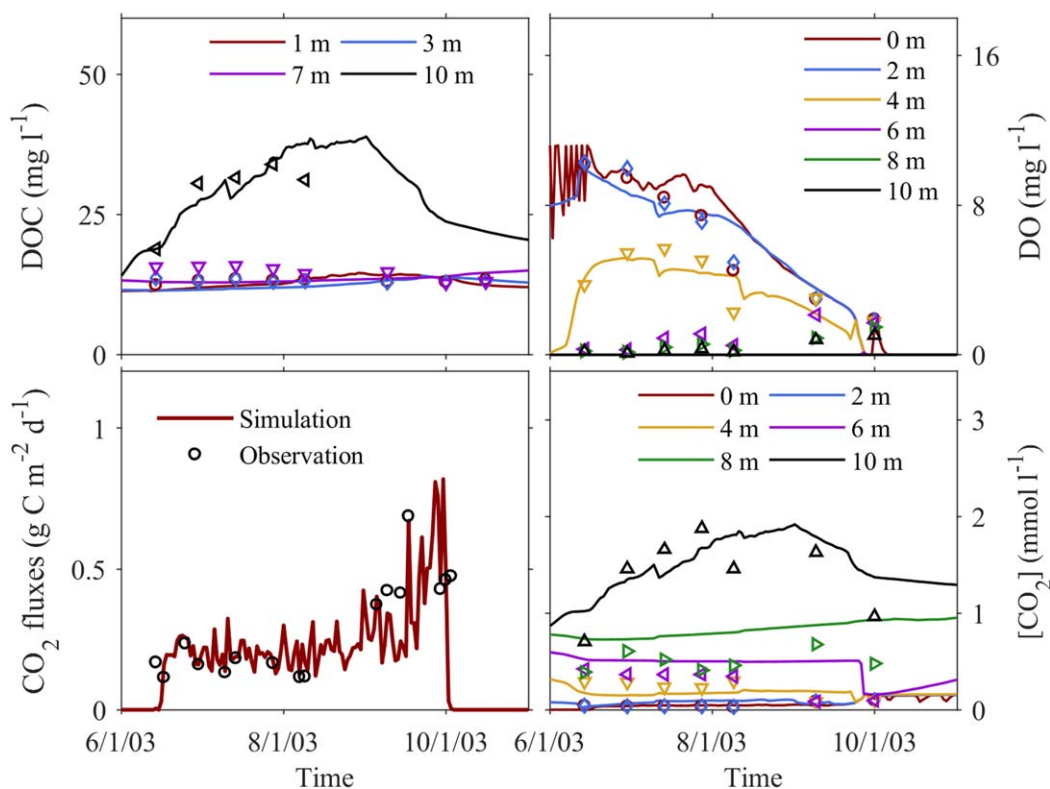


Figure 6. Dynamics of DOC, dissolved O₂ (DO), dissolved CO₂, and CO₂ fluxes at Shuchi Lake from 1 June 2003 to 1 November 2003. Symbols represent the observed values and lines represent the simulated values.

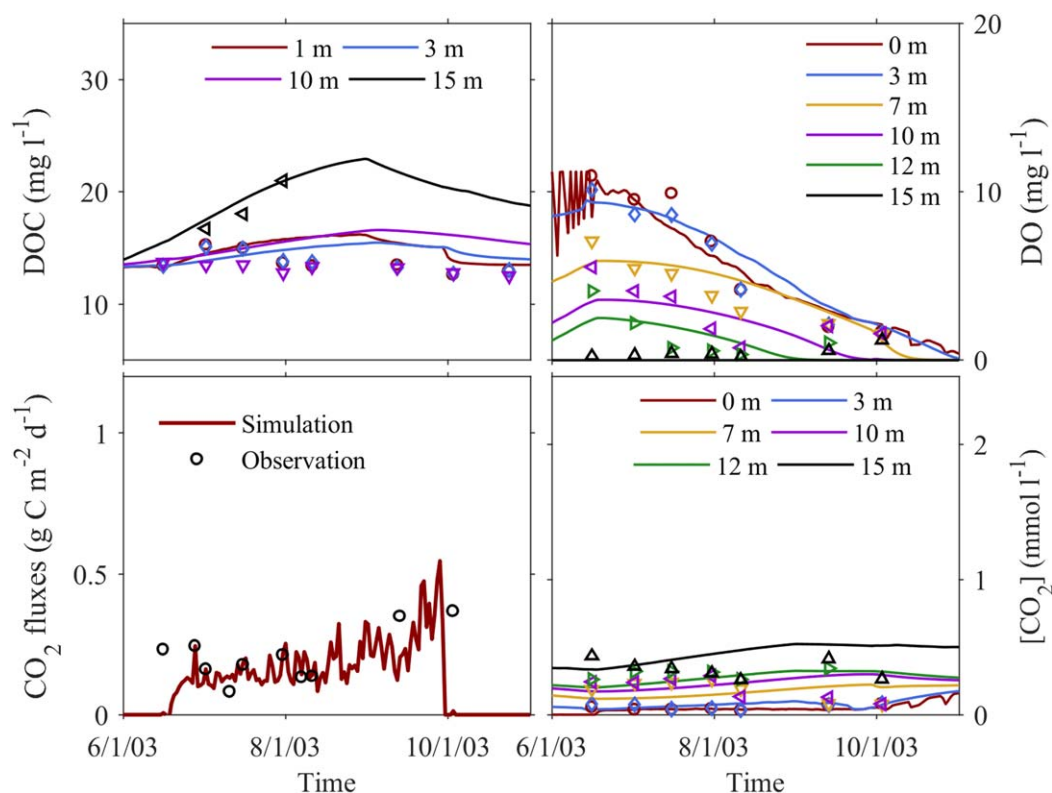


Figure 7. Dynamics of DOC, dissolved O₂ (DO), dissolved CO₂, and CO₂ fluxes at Tube Dispenser Lake from 1 June 2003 to 1 November 2003. Symbols represent the observed values and lines represent the simulated values.

surface reaeration) and O₂ loss (through respiration), the reproduction of dissolved O₂ (Figures 6–8) cannot guarantee the good simulation of primary production if surface reaeration and/or respiration are uncertain. During the summer periods without deep water mixing, surface reaeration of these small lakes is usually very weak due to wind sheltering [Markfort *et al.*, 2010]. Thus, if the simulated respiration is well constrained, the simulated dynamics of chlorophyll *a* will be validated. Here we do not have observations to validate the simulated respiration. But as DOC and DIC in lake waters are dominated by autotrophic and heterotrophic respiration and the ALBM reproduces their levels at different depths (Figures 6–8), it is likely that both the simulated primary production and respiration are reasonable.

3.2.3. Russian Thermokarst Lakes

During the open-water seasons of 2007–2008, the simulated mean daily CO₂ fluxes from the two Russian thermokarst lakes, Seida A and B Lake, are 0.19 and 0.10 g C m⁻² d⁻¹, respectively, and the observed mean daily CO₂ fluxes from the two lakes are 0.36 and 0.10 g C m⁻² d⁻¹, respectively (Figure 9). For Seida A Lake, there were some extraordinarily high CO₂ fluxes in the later summers of 2007–2008 that our model failed to reproduce. It accounts for the large discrepancy between the simulated and observed CO₂ fluxes at this lake. The high observed CO₂ fluxes might be driven by DOC and DIC inputs from the water flow which are not well resolved by the VIC-based monthly runoff data. According to Ledesma *et al.* [2015], the storm-induced carbon load can increase the water-column stocks of DOC and DIC of very small lakes dramatically. In addition, the model performance might also be improved by refining the representation of violent turbulence in shallow lakes [Jonas *et al.*, 2003; Laurion *et al.*, 2010]. But as these outbursts of CO₂ fluxes were not observed from Seida B Lake, the abrupt changes of boundary conditions might not be able to fully explain the observed flux outbursts. Further studies are needed to understand the underlying mechanisms. The modeled CO₂ fluxes from the two thermokarst lakes have interannual variations: (1) the mean daily CO₂ fluxes from Seida A Lake during the open-water periods of 2007 and 2008 are 0.17 and 0.20 g C m⁻² d⁻¹, respectively and (2) the mean daily CO₂ fluxes from Seida B Lake during the open-water periods of 2007 and 2008 are 0.10 and 0.11 g C m⁻² d⁻¹, respectively. The higher CO₂ fluxes in 2008 may be explained by the lower buoyancy fluxes and larger turbulence of the lakes in the year, which were driven by the lower temperature and solar radiation.

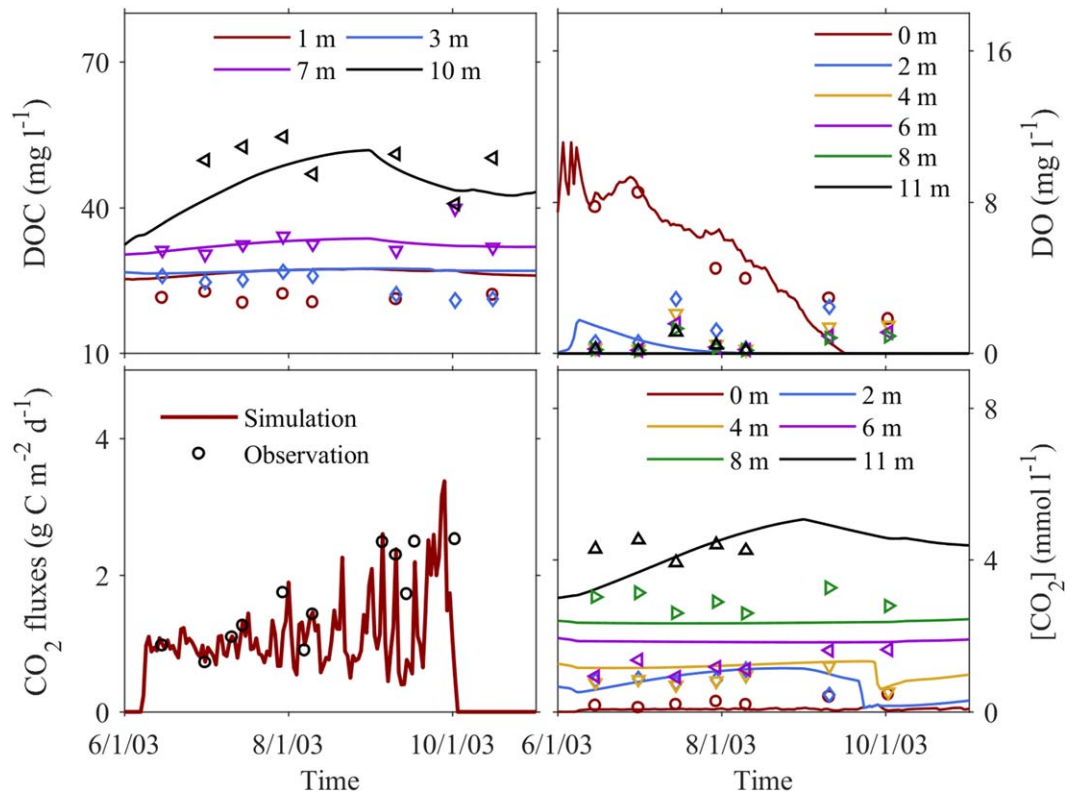


Figure 8. Dynamics of DOC, dissolved O₂, dissolved CO₂ (DO), and CO₂ fluxes at Grass Lake from 1 June 2003 to 1 November 2003. Symbols represent the observed values and lines represent the simulated values.

In the Seida lakes, chlorophyll *a* concentrations peaked in the middle of July when strong convective mixing just waned. The maximum areal-specific chlorophyll *a* during the open-water seasons of 2007 and 2008 are 5.2 and 1.9 mg m⁻², respectively, in Seida A Lake and 0.94 and 0.75 mg m⁻², respectively, in Seida B Lake. The mean areal-specific chlorophyll *a* during the open-water seasons of 2007 and 2008 are 2.9 and 1.3 mg m⁻², respectively, in Seida A Lake and 0.50 and 0.41 mg m⁻², respectively, in Seida B Lake. The simulated

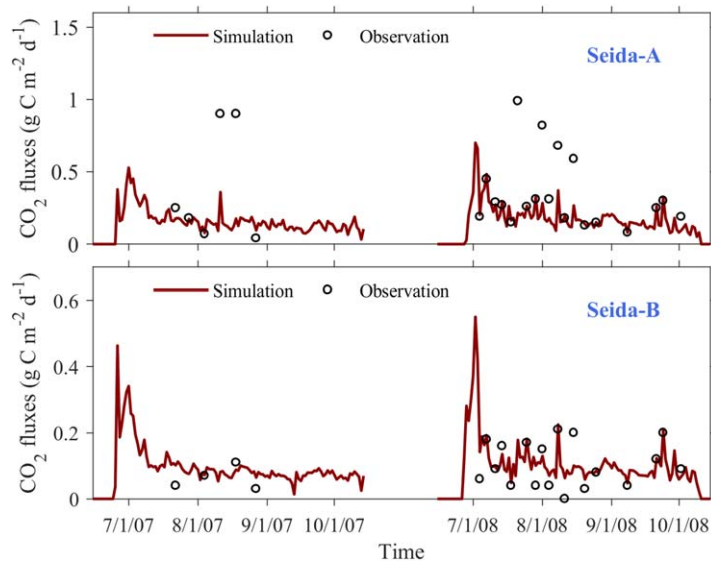


Figure 9. Dynamics of CO₂ fluxes at Seida A and B Lake from 15 June 2007 to 15 October 2007 and from 15 June 2008 to 15 October 2008.

primary production, mineralization and respiration will be discussed in detail in section 3.4. Unlike Toolik Lake and the yedoma lakes, we do not have the related observations to validate these simulations for the two thermokarst lakes, which introduces additional uncertainties to our simulations.

3.3. Whole-Lake Carbon Balance

Because the carbon dynamics of Arctic lakes involve many processes which could interact with each other and vary both temporally and spatially, analyzing the whole-lake carbon balance for Arctic lakes can be difficult with field or laboratory

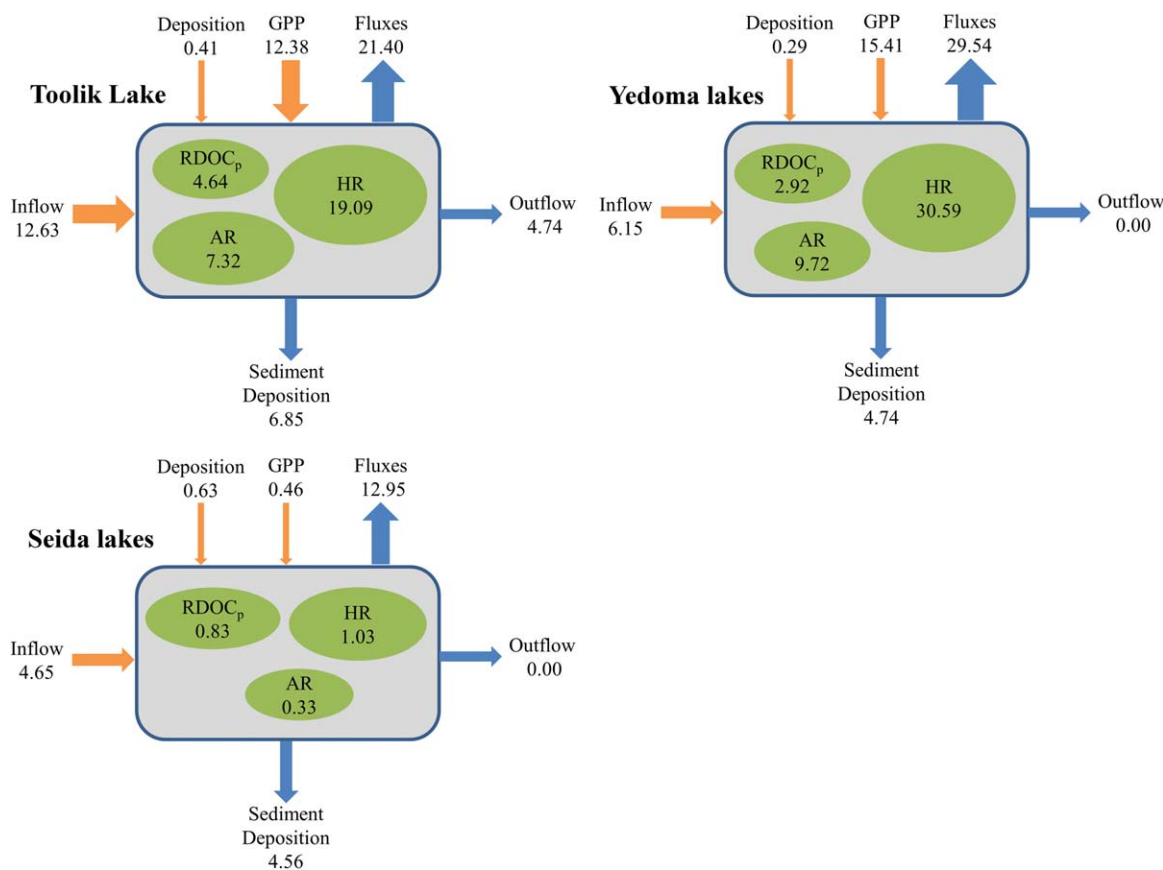


Figure 10. Whole-lake carbon balance of the glacial lake (Toolik Lake), the Siberian yedoma lakes, and the Russian thermokarst lakes (Seida lakes). The analysis includes the area-weighted values ($\text{g C m}^{-2} \text{ yr}^{-1}$) of carbon loads from surface and subsurface water inflow (inflow), carbon loss from surface water outflow (outflow), carbon dry and wet air deposition (deposition), gross primary production (GPP), CO_2 fluxes (fluxes), carbon sediment deposition, DOC photomineralization ($RDOC_p$), autotrophic respiration (AR), and heterotrophic respiration (HR) including biomineralization and methanotrophy.

experiments and previous simpler biogeochemistry models. The analysis is straightforward using the ALBM (Figure 10). Our analysis indicates that all the study lakes are CO_2 sources to the atmosphere (Figure 10). Because heterotrophic respiration in the yedoma lakes is fueled by the leaching and mobilization of labile OC from land and taliks [Vonk *et al.*, 2013; Walter Anthony *et al.*, 2014; Sepulveda-Jauregui *et al.*, 2015; Spencer *et al.*, 2015], CO_2 fluxes from the yedoma lakes are the highest at $29.54 \text{ g C m}^{-2} \text{ yr}^{-1}$. It should be noted that there is a large amount of carbon flux from sediments to the water body in yedoma lakes ($12.43 \text{ g C m}^{-2} \text{ yr}^{-1}$), a fraction of which could support the high CO_2 fluxes at the surface. In the study, we did not account for small amounts of carbon outflow from the outlets of Shuchi Lake and Tube Dispenser Lake because of the lack of water flow measurements. The exclusion of this carbon sink can cause heterotrophic respiration in these two lakes underestimated. Because Seida B Lake has low CO_2 fluxes but is much larger than Seida A Lake, the area-weighted annual CO_2 fluxes from the thermokarst lakes are small at $12.95 \text{ g C m}^{-2} \text{ yr}^{-1}$. It was documented that at different evolution stages there could be considerable changes of water biogeochemistry in thermokarst lakes [Manasypov *et al.*, 2017]. Thus, the contribution of thermokarst lakes to the global carbon cycle may depend on which stage of thermokarst lakes dominates in total area. Similar to the yedoma lakes, there are also high carbon fluxes ($11.77 \text{ g C m}^{-2} \text{ yr}^{-1}$) from sediments to water in the thermokarst lakes. The analysis of Toolik Lake implies that among the study lake types, glacial lakes may contribute the largest amount of CO_2 fluxes in the Arctic, due to their dominance in lake area [Wetzel, 2001; Wik *et al.*, 2016] and comparable area-specific CO_2 fluxes ($21.4 \text{ g C m}^{-2} \text{ yr}^{-1}$). In comparison with the yedoma lakes and thermokarst lakes, in Toolik Lake, biomineralization and carbon loading have comparable roles in maintaining CO_2 fluxes and the carbon fluxes at the water-sediment interface are much smaller at $7.57 \text{ g C m}^{-2} \text{ yr}^{-1}$.

There are interesting findings for the role of photochemical mineralization in the carbon balance of Arctic lakes from the model: the absolute amount of photomineralization is larger in deep lakes (e.g., Toolik Lake), but on the contrary the relative role of photomineralization is larger in shallow lakes (e.g., the Seida lakes). The first difference should be mainly attributed to the different light usage ratios between deep and shallow lakes. In the water column of deep lakes, almost all UV radiation can be absorbed through CDOM degradation. But in the water column of very shallow lakes, only a fraction of UV can be absorbed due to short light paths and the rest of UV would be absorbed by dark sediments. And the second difference should be mainly attributed to the attenuation of UV in the water column with depth. As a result, on average, shallow water CDOM would be exposed to more intense UV. These results support the claim of *Cory et al.* [2014] that photomineralization accounts for more DOC degradation in shallow Arctic lakes. However, the analysis also implies that the overall contribution of photomineralization to the carbon balance of Arctic lakes could be limited due to the limitation of UV energy. Because of the low photolability of yedoma permafrost carbon [Stubbins et al., 2017], the absolute photomineralization rate of the yedoma lakes is smaller than that of Toolik Lake.

Carbon burial in lake sediments is an important carbon sink in the global carbon cycle, on the magnitude larger than carbon burial in ocean sediments [Ward et al., 2017]. But the understanding for carbon burial in the sediments of Arctic lakes is still uncertain [Sobek et al., 2009, 2014]. Because the DOC trapped in ice layers is removed in the model and the shallow thermokarst lakes have relatively larger proportions of ice layers, the ALBM predicts relatively higher carbon deposition rates in the thermokarst lakes (Figure 10). The long-term OC accumulation rate in Siberian yedoma lakes was reported at around $45 \text{ g C m}^{-2} \text{ yr}^{-1}$ [Walter Anthony et al., 2014], which is much larger than the simulated value here. As it was suggested that much of the sediment OC is from terrestrial particulate OC sources and the primary production of benthic mosses [Walter Anthony et al., 2014], the ALBM may need to represent these two carbon sources to accurately estimate carbon burial in lake sediments.

4. Limitations

Similar to other biogeochemistry models, we have to make some assumptions to simplify the complex biogeochemical processes of Arctic lakes in the model development. These assumptions may introduce an additional level of uncertainty to model simulations, especially for some processes sensitive to certain assumptions. For example, for Arctic lakes without inlet streams, phytoplankton primary production and DOC mineralization can be sensitive to the leaching of land OC (Figure 3). Because most of the DOC leaching in the Arctic could occur only in top soils [Godsey et al., 2009; Ledesma et al., 2015] and vary with the changes of climate and terrestrial ecosystem phenology [Einarsdottir et al., 2017], the use of a constant subsurface DOC concentration parameter (DOC_{gw}) may not well resolve the carbon load's temporal variability. Further, because DOC can be converted to DIC by mineralization in lakes, it is difficult to constrain the two carbon loads separately using the data from lake water samples. As a result, the model now assumes that the DIC leaching is equal to one quarter of the DOC leaching and compensates the overestimate or underestimate of the DIC leaching by adjusting DOC mineralization. But this assumption may be inappropriate because the ratio of DOC to DIC in subsurface water flow was found to vary largely [Einarsdottir et al., 2017]. To better represent the dynamics of external carbon inputs, it will be necessary in the future to drive the DOC and DIC leaching using a terrestrial ecosystem model, such as the terrestrial ecosystem model (TEM) [Zhuang et al., 2003, 2010], which represents high-latitude hydrology and carbon dynamics [Liu et al., 2014; Lu and Zhuang, 2015]. The coupling of the ALBM and a terrestrial ecosystem model can be useful for a comprehensive assessment of the Arctic carbon balance involving both land and inland water landscapes. Similarly, instead of using a constant thermokarst erosion rate (r_{thaw}), a more complex scheme to represent thermokarst erosion and the corresponding changes of OC stocks in sediments may be needed for the ALBM to better simulate OC mineralization in taliks [Tan and Zhuang, 2015a]. For OC deposition to sediments, the use of the same deposition rate for all lakes could be an oversimplification. Several studies have shown that carbon deposition could be related to pH and iron concentrations [Shirokova et al., 2013; Manasyrov et al., 2015] that vary among lakes. Additionally, the model may also need to represent terrestrial particulate OC loading and the primary production of benthic mosses to realistically simulate OC deposition to sediments. Possibly, it is also necessary to include more phytoplankton functional groups and nitrogen limitation to photosynthesis to better represent the evolution of aquatic ecosystems under changing

environmental conditions [Chambers, 1987; Hipsey and Hamilton, 2008]. Additionally, the model may need to represent the C:P ratios in the POM and DOM of Arctic lakes dynamically as described in the CAEDYM model [Hipsey and Hamilton, 2008] to better simulate the nutrient limitation on phytoplankton growth because fixed C:P stoichiometry is not fully consistent with the observations [Prater *et al.*, 2017].

Besides the above oversimplifications, as discussed before, the model performance can also be limited by the use of low-resolution boundary and hydrological conditions (such as CERES, ECMWF, and VIC) and the lack of storm-induced carbon load. Especially, the reliability of using the VIC runoff data to drive the hydrological carbon inputs of small lakes in the Arctic has not been tested. Several efforts have been made in this study to constrain the hydrological carbon inputs, including the use of published data to constrain the sub-surface flow of Toolik Lake and the simulation of the carbon inputs at the monthly scale. However, it is likely that there are still large uncertainties in the estimates due to the coarse resolution of the data. Further, the use of monthly water flow also makes storm-induced carbon load unresolved in the model. Thus, it will be valuable in the future study to couple the ALBM with a fine-scale hydrological model specific to the Arctic regions to study the influence of external carbon inputs on the carbon dynamics of Arctic lakes.

As discussed before, the accuracy of the model simulations can also be limited by the quality of the observations. First, because the observed CO₂ fluxes were measured by three different methods which are not always consistent in predicting the temporal variability of CO₂ outgassing, the model evaluation could have a certain degree of systematic uncertainty. Especially, the data of CO₂ fluxes for the yedoma and Seida lakes are actually not direct measured fluxes but also modeled fluxes based on surface CO₂ concentrations and gas transfer velocity. This means that the data have two uncertainty sources: the measurements and the estimates of gas transfer velocity. Second, because of the lack of data, some of the simulated processes have not been evaluated fully. Especially, we have not tested the simulated photomineralization rates in the Seida lakes which as shown in the results could be substantial. To improve our understanding of this topic, it will be necessary for experimental scientists to interact with modeling scientists to optimize their experimental design before the start of a field survey. It will also be necessary for experimental scientists to conduct joint field campaigns on different Arctic lakes with standardized measurement methods.

5. Conclusions

This study developed a one-dimensional process-based lake biogeochemistry model (ALBM) that explicitly simulates the dynamics of POC, DOC, and DIC in the water and sediment columns to estimate CO₂ fluxes from different Arctic lakes, especially the vast number of small lakes in the Arctic [Holgerson and Raymond, 2016]. In comparison with existing lake biogeochemistry models [Hipsey and Hamilton, 2008; Stepanenko *et al.*, 2016], the ALBM includes several important processes for CO₂ fluxes, e.g., carbon mineralization by photochemistry, carbon mineralization in sediments, carbon mobilization from thawing permafrost, and energy and carbon exchanges at the water-sediment interface. The simulated area-weighted CO₂ fluxes from yedoma lakes, thermokarst lakes and a glacial lake are 29.5, 13.0, and 21.4 g C m⁻² yr⁻¹, respectively, close to the observed values (31.2, 17.2, and 16.5 ± 7.7 g C m⁻² yr⁻¹, respectively). Through considering the OC stock induced by thermokarst erosion and the lability of yedoma permafrost OC, the model can better simulate high CO₂ fluxes from yedoma lakes. Because of the integrated biogeochemical processes and the well-simulated thermal dynamics, the ALBM can reproduce the seasonal variations of CO₂ fluxes from the study lakes. This model also includes different parameterizations for the growth, metabolism, nutrient limitation, and movement of different freshwater phytoplankton. As a result, it shows good performance in simulating phytoplankton primary production and chlorophyll *a* concentrations in Toolik Lake. Using the ALBM, the analysis of the whole-lake carbon balance can be straightforward. Our analysis indicates that although the relative contribution of photomineralization to the carbon balance of shallow Arctic lakes could be particularly large, its overall contribution to the global carbon cycle could be limited due to the constraint of UV energy. Our analysis also identifies clear differences between glacial, thermokarst, and yedoma lakes in autotrophic and heterotrophic respiration and OC sedimentation. Overall, our analysis indicates that the ABLM model can simulate the changes of CO₂ fluxes from Arctic lakes that differ in morphology, permafrost carbon, land cover, hydrology, and climate, which were rarely calculated by previous lake biogeochemistry models. Importantly, by the upgrade, the ALBM includes all essential processes to quantify the dynamics of both CO₂ and CH₄ in Arctic lakes.

Acknowledgments

We thank European Center for providing Medium-Range Weather Forecasts (ECMWF) Interim re-analysis (ERA-Interim), Bolin Centre Database for providing the Northern Circumpolar Soil Carbon Database, NASA Goddard Space Flight Center for providing SeaWiFS Deep Blue Aerosol Optical Depth data sets, Max-Planck Institute for providing MAC-v2 data sets, and World Radiation Monitoring Center for the BSRN data sets. We also thank the Arctic LTER project for maintaining the Toolik Lake field observations (NFS-1107593). ArcticDEM for this work is provided by the Polar Geospatial Center under NSF OPP awards 1043681 and 1559691. This study is supported through projects funded to Q.Z. by the NASA Land Use and Land Cover Change program (NASA-NNX09A126G), Department of Energy (DE-FG02-08ER64599), the NSF Division of Information and Intelligent Systems (NSF-1028291), the NSF Carbon and Water in the Earth program (NSF-0630319), the USGS (G17AC00276) and to K.W.A. by NSF ARC-1304823 and NSF OPP #1107892. This research is also in part supported by the Director, Office of Science, Office of Biological and Environmental Research of the US Department of Energy under contract DE-AC02-05CH11231 as part of their Earth System Modeling Program. The data presented in this study will be deposited to our research laboratory website (www.purdue.edu/eaps/ebdl) to allow the public to access.

References

- Aberg, J., M. Jansson, and A. Jonsson (2010), The importance of water temperature and thermal stratification dynamics for temporal variation of surface water CO₂ in a boreal lake, *J. Geophys. Res.*, *115*, G02024, doi:10.1029/2009JG001085.
- Arp, C. D., B. M. Jones, G. Grosse, A. C. Bondurant, V. E. Romanovsky, K. M. Hinkel, and A. D. Parsekian (2016), Threshold sensitivity of shallow Arctic lakes and sublake permafrost to changing winter climate, *Geophys. Res. Lett.*, *43*, 6358–6365, doi:10.1002/2016GL068506.
- Aufdenkampe, A. K., E. Mayorga, P. A. Raymond, J. M. Melack, S. C. Doney, S. R. Alin, R. E. Aalto, and K. Yoo (2011), Riverine coupling of biogeochemical cycles between land, oceans, and atmosphere, *Front. Ecol. Environ.*, *9*, 53–60, doi:10.1890/100014.
- Bertilsson, S., and L. Tranvik (2000), Photochemical transformation of dissolved organic matter in lakes, *Limnol. Oceanogr.*, *45*(4), 753–762.
- Boers, R., M. J. de Haij, W. M. F. Wauben, H. K. Baltink, L. H. van Ulf, M. Savenije, and C. N. Long (2010), Optimized fractional cloudiness determination from five ground-based remote sensing techniques, *J. Geophys. Res.*, *115*, D24116, doi:10.1029/2010JD014661.
- Buffam, I., M. G. Turner, A. R. Desai, P. C. Hanson, J. A. Rusak, N. R. Lottig, E. H. Stanley, and S. R. Carpenter (2011), Integrating aquatic and terrestrial components to construct a complete carbon budget for a north temperate lake district, *Global Change Biol.*, *17*, 1193–1211, doi:10.1111/j.1365-2486.2010.02313.x.
- Burd, A. B., et al. (2015), Terrestrial and marine perspectives on modeling organic matter degradation pathways, *Global Change Biol.*, *22*, 121–136, doi:10.1111/gcb.12987.
- Campolongo, F., J. Cariboni, and A. Saltelli (2007), An effective screening design for sensitivity analysis of large models, *Environ. Modell. Software*, *22*, 1509–1518.
- Chambers, P. A. (1987), Light and nutrients in the control of aquatic plant community structure. II. In situ observations, *J. Ecol.*, *75*, 621–628.
- Cole, J. J., et al. (2007), Plumbing the global carbon cycle: Integrating inland waters into the terrestrial carbon budget, *Ecosystems*, *10*, 172–185, doi:10.1007/s10021-006-9013-8.
- Cory, R. M., B. C. Crump, J. A. Dobkowski, and G. W. Kling (2013), Surface exposure to sunlight stimulates CO₂ release from permafrost soil carbon in the Arctic, *Proc. Natl. Acad. Sci. U. S. A.*, *110*, 3429–3434, doi:10.1073/pnas.1214104110.
- Cory, R. M., C. P. Ward, B. C. Crump, and G. W. Kling (2014), Sunlight controls water column processing of carbon in Arctic fresh waters, *Science*, *345*, 925–928, doi:10.1126/science.1253119.
- Crump, B. C., G. W. Kling, M. Bahr, and J. E. Hobbie (2003), Bacterioplankton community shifts in an Arctic lake correlate with seasonal changes in organic matter source, *Appl. Environ. Microbiol.*, *69*, 2253–2268, doi:10.1128/AEM.69.4.2253-2268.2003.
- Daniels, W. C., G. W. Kling, and A. E. Giblin (2015), Benthic community metabolism in deep and shallow Arctic lakes during 13 years of whole-lake fertilization, *Limnol. Oceanogr.*, *60*, 1604–1618, doi:10.1002/lno.10120.
- Dee, D. P., and S. Uppala (2009), Variational bias correction of satellite radiance data in the ERA-Interim reanalysis, *Q. J. R. Meteorol. Soc.*, *135*, 1830–1841.
- DeFries, R., M. Hansen, J. R. G. Townshend, A. C. Janetos, and T. R. Loveland (2000), A new global 1 km data set of percent tree cover derived from remote sensing, *Global Change Biol.*, *6*, 247–254.
- Deshpande, B. N., S. MacIntyre, A. Matveev, and W. F. Vincent (2015), Oxygen dynamics in permafrost thaw lakes: Anaerobic bioreactors in the Canadian subarctic, *Limnol. Oceanogr.*, *60*, 1656–1670, doi:10.1002/lno.10126.
- Downing, J. A., Y. T. Prairie, J. J. Cole, C. M. Duarte, L. J. Tranvik, R. G. Striegl, W. H. McDowell, P. Kortelainen, N. F. Caraco, and J. M. Melack (2006), The global abundance and size distribution of lakes, ponds, and impoundments, *Limnol. Oceanogr.*, *51*, 2388–2397.
- Drake, T. W., K. P. Wickland, R. G. M. Spencer, D. M. McKnight, and R. G. Striegl (2015), Ancient low-molecular-weight organic acids in permafrost fuel rapid carbon dioxide production upon thaw, *Proc. Natl. Acad. Sci. U. S. A.*, *112*, 13,946–13,951, doi:10.1073/pnas.1511705112.
- Dutton, E. G. (2007), *Basic and other measurements of radiation at station Barrow (2001–2004)*, Clim. Monit. & Diagn. Lab., Boulder, Colo., doi:10.1594/PANGAEA.668523.
- Einarsdottir, K., M. B. Wallin, and S. Sobek (2017), High terrestrial carbon load via groundwater to a boreal lake dominated by surface water inflow, *J. Geophys. Res. Biogeosci.*, *122*, 15–29, doi:10.1002/2016JG003495.
- Environmental Data Center Team (2016), *Meteorological Monitoring Program at Toolik, Alaska*, Toolik Field Stn., Inst. of Arctic Biol., Univ. of Alaska Fairbanks, Fairbanks. [Available at http://toolik.alaska.edu/edc/abiotic_monitoring/data_query.php.]
- Eugster, W., G. Kling, T. Jonas, J. P. McFadden, A. Wüest, S. MacIntyre, and F. S. Chapin III (2003), CO₂ exchange between air and water in an Arctic Alaskan and midlatitude Swiss lake: Importance of convective mixing, *J. Geophys. Res.*, *108*(D12), 4362, doi:10.1029/2002JD002653.
- Evans, C. D., D. T. Monteith, and D. M. Cooper (2005), Long-term increases in surface water dissolved organic carbon: Observations, possible causes and environmental impacts, *Environ. Pollut.*, *137*, 57–71, doi:10.1016/j.envpol.2004.12.031.
- Fichot, C. G., and W. L. Miller (2010), An approach to quantify depth-resolved marine photochemical fluxes using remote sensing: Application to carbon monoxide (CO) photoproduction, *Remote Sens. Environ.*, *114*, 1363–1377, doi:10.1016/j.rse.2010.01.019.
- Giblin, A. (2006), *Corrected Chlorophyll a Data for Toolik Lake and Surrounding Lakes Near the Arctic LTER Site During the Summer of 2014*, Long Term Ecol. Res. Network, Santa Barbara, Calif., doi:10.6073/pasta/ca4bbc719f15e3fec66ac709d8bb880bd.
- Giblin, A., C. Luecke, and G. Kling (2005), *Physical and Chemical Data for Various Lakes Near Toolik Research Station, Arctic LTER Summer 2014*, Long Term Ecol. Res. Network, Santa Barbara, Calif., doi:10.6073/pasta/f841d0c652be753a794357ae6b198ed2.
- Giblin, A., C. Luecke, and G. Kling (2010), *Nutrient and Chemical Data for Various Lakes Near Toolik Research Station, Arctic LTER, Summer 2014*, Long Term Ecol. Res. Network, Santa Barbara, Calif., doi:10.6073/pasta/2f4f29e0736d34e77e7def7278fe711.
- Godsey, S. E., J. W. Kirchner, and D. W. Clow (2009), Concentration–discharge relationships reflect chemostatic characteristics of US catchments, *Hydrol. Processes*, *23*, 1844–1864, doi:10.1002/hyp.7315.
- Grant, R. H., and W. Gao (2003), Diffuse fraction of UV radiation under partly cloudy skies as defined by the Automated Surface Observation System (ASOS), *J. Geophys. Res.*, *108*(D2), 4046, doi:10.1029/2002JD002201.
- Greene, S., K. M. Walter Anthony, D. Archer, A. Sepulveda-Jauregui, and K. Martinez-Cruz (2014), Modeling the impediment of methane ebullition bubbles by seasonal lake ice, *Biogeosciences*, *11*, 6791–6811, doi:10.5194/bg-11-6791-2014.
- Groenewald, M., L. Tranvik, S. Natchimuthu, and B. Koehler (2016), Photochemical mineralisation in a boreal brown water lake: Considerable temporal variability and minor contribution to carbon dioxide production, *Biogeosciences*, *13*, 3931–3943, doi:10.5194/bg-13-3931-2016.
- Gueymard, C. (1995), SMARTS2, Simple Model of the Atmospheric Radiative Transfer of Sunshine: Algorithms and performance assessment, *Rep. FSEC-PF-270-95*, Fla. Sol. Energy Cent., Cocoa.
- Gueymard, C. (2005), Interdisciplinary applications of a versatile spectral solar irradiance model: A review, *Energy*, *30*, 1551–1576.
- Hanson, P. C., A. I. Pollard, D. L. Bade, K. Predick, S. R. Carpenter, and J. A. Foley (2004), A model of carbon evasion and sedimentation in temperate lakes, *Global Change Biol.*, *10*, 1285–1298.
- Hanson, P. C., D. P. Hamilton, E. H. Stanley, N. Preston, O. C. Langman, and E. L. Kara (2011), Fate of allochthonous dissolved organic carbon in lakes: A quantitative approach, *PLoS One*, *6*, e21884, doi:10.1371/journal.pone.0021884.

- Hanson, P. C., I. Buffam, J. A. Rusak, E. H. Stanley, and C. Watras (2014), Quantifying lake allochthonous organic carbon budgets using a simple equilibrium model, *Limnol. Oceanogr.*, *59*, 167–181, doi:10.4319/lo.2014.59.01.0167.
- Heiskanen, J. J., I. Mammarella, S. Haapanala, J. Pumpanen, T. Vesala, S. Macintyre, and A. Ojala (2014), Effects of cooling and internal wave motions on gas transfer coefficients in a boreal lake, *Tellus, Ser. B*, *66*, 22827, doi:10.3402/tellusb.v66.22827.
- Hipsey, M. R., and D. P. Hamilton (2008), *Computational Aquatic Ecosystem Dynamic Model: CAEDYM v3 Science Manual*, Cent. for Water Res. Rep., Univ. of West. Aust., Nedlands, Australia.
- Holgerson, M. A., and P. A. Raymond (2016), Large contribution to inland water CO₂ and CH₄ emissions from very small ponds, *Nat. Geosci.*, *9*, 222–226, doi:10.1038/ngeo2654.
- Hopkinson, C. S., and J. J. Vallino (2005), Efficient export of carbon to the deep ocean through dissolved organic matter, *Nature*, *433*, 142–145.
- Jäger, C. G., and S. Diehl (2014), Resource competition across habitat boundaries: Asymmetric interactions between benthic and pelagic producers, *Ecol. Monogr.*, *84*, 287–302, doi:10.1890/13-0613.1.
- Jonas, T., A. Stips, W. Eugster, and A. Wüest (2003), Observations of a quasi shear-free lacustrine convective boundary layer: Stratification and its implications on turbulence, *J. Geophys. Res.*, *108*(C10), 3328, doi:10.1029/2002JC001440.
- Jones, B. M., G. Grosse, C. D. Arp, M. C. Jones, K. M. Walter Anthony, and V. E. Romanovsky (2011), Modern thermokarst lake dynamics in the continuous permafrost zone, northern Seward Peninsula, Alaska, *J. Geophys. Res.*, *116*, G00M03, doi:10.1029/2011JG001666.
- Kallis, A. (2007), *Basic and Other Measurements of Radiation at Station Toravere (2001–2004)*, Tartu Obs., Toravere, Estonia, doi:10.1594/PANGAEA.671373.
- Kasten, F., and G. Czeplak (1980), Solar and terrestrial radiation dependent on the amount and type of cloud, *Solar Energy*, *24*, 177–189.
- Kellerman, A. M., D. N. Kothawala, T. Dittmar, and L. J. Tranvik (2015), Persistence of dissolved organic matter in lakes related to its molecular characteristics, *Nat. Geosci.*, *8*, 454–457, doi:10.1038/ngeo2440.
- Kinne, S., D. O'Donnell, P. Stier, S. Kloster, K. Zhang, H. Schmidt, S. Rast, M. Giorgetta, T. F. Eck, and B. Stevens (2013), MAC-v1: A new global aerosol climatology for climate studies, *J. Adv. Model. Earth Syst.*, *5*, 704–740, doi:10.1002/jame.20035.
- Kirk, J. T. O. (2011), *Light and Photosynthesis in Aquatic Ecosystems*, 3rd ed., Cambridge Univ. Press, Cambridge, U. K.
- Kling, G. W. (2005), *Toolik Inlet Discharge Data Collected in Summer 2014, Arctic LTER, Toolik Research Station, Alaska*, Long Term Ecol. Res. Network, Santa Barbara, Calif., doi:10.6073/pasta/Off1200625faacb3c14426437bed9199.
- Kling, G. W. (2010), *Primary Production Data for Lakes and Lake Inlets/Outlets Samples Collected Summer 2014, Arctic LTER, Toolik Research Station, Alaska*, Long Term Ecol. Res. Network, Santa Barbara, Calif., doi:10.6073/pasta/b979944424bfa3ee58f82db2a798db0e.
- Kling, G. W., G. W. Kipphut, and M. C. Miller (1991), Arctic lakes and streams as gas conduits to the atmosphere: Implications for tundra carbon budgets, *Science*, *251*(4991), 298–301.
- Kling, G. W., W. J. O'Brien, M. C. Miller, and A. E. Hershey (1992), The biogeochemistry and zoogeography of lakes and rivers in Arctic Alaska, *Hydrobiologia*, *240*, 1–14.
- Kling, G. W., G. W. Kipphut, M. M. Miller, and W. J. O'Brien (2000), Integration of lakes and streams in a landscape perspective: The importance of material processing on spatial patterns and temporal coherence, *Freshwater Biol.*, *43*(3), 477–497.
- Koehler, B., T. Landelius, G. A. Weyhenmeyer, N. Machida, and L. J. Tranvik (2014), Sunlight-induced carbon dioxide emissions from inland waters, *Global Biogeochem. Cycles*, *28*, 696–711, doi:10.1002/2014GB004850.
- Kromkamp, J., and A. E. Walsby (1990), A computer model of buoyancy and vertical migration in cyanobacteria, *J. Plankton Res.*, *12*, 161–183.
- Langer, M., S. Westermann, K. Walter Anthony, K. Wischniewski, and J. Boike (2015), Frozen ponds: Production and storage of methane during the Arctic winter in a lowland tundra landscape in northern Siberia, Lena River delta, *Biogeosciences*, *12*, 977–990, doi:10.5194/bg-12-977-2015.
- Laurion, I., W. Vincent, S. MacIntyre, L. Retamal, C. Dupont, P. Francus, and R. Pienitz (2010), Variability in greenhouse gas emissions from permafrost thaw ponds, *Limnol. Oceanogr.*, *55*, 115–133, doi:10.4319/lo.2010.55.1.0115.
- Ledesma, J. L. J., T. Grabs, K. H. Bishop, S. L. Schiff, and S. J. Köhler (2015), Potential for long-term transfer of dissolved organic carbon from riparian zones to streams in boreal catchments, *Global Change Biol.*, *21*, 2963–2979, doi:10.1111/gcb.12872.
- Lee, H., E. A. G. Schuur, K. S. Inglett, M. Lavoie, and J. P. Chanton (2012), The rate of permafrost carbon release under aerobic and anaerobic conditions and its potential effects on climate, *Global Change Biol.*, *18*(2), 515–527, doi:10.1111/j.1365-2486.2011.02519.x.
- Lewis, W. M. (2011), Global primary production of lakes: 19th Baldi Memorial Lecture, *Int. Waters*, *1*, 1–28, doi:10.5268/IW-1.1.384.
- Li, Q. P., P. J. S. Franks, M. R. Landry, R. Goericke, and A. G. Taylor (2010), Modeling phytoplankton growth rates and chlorophyll to carbon ratios in California coastal and pelagic ecosystems, *J. Geophys. Res.*, *115*, G04003, doi:10.1029/2009JG001111.
- Liu, Y., Q. Zhuang, Z. Pan, D. Miralles, N. Tchekabakova, D. Kicklighter, J. Chen, A. Sirin, Y. He, and G. Zhou (2014), Response of evapotranspiration and water availability to the changing climate in Northern Eurasia, *Clim. Change*, *126*, 413–427.
- Lu, X., and Q. Zhuang (2015), An integrated Dissolved Organic Carbon Dynamics Model (DOCMD 1.0): Model development and a case study in the Alaskan Yukon River Basin, *Geosci. Model Dev. Discuss.*, *8*, 10,411–10,454, doi:10.5194/gmdd-8-10411-2015.
- MacIntyre, S. (1998), Turbulent mixing and resource supply to phytoplankton, in *Physical Processes in Lakes and Oceans, Coastal Estuarine Stud.*, vol. 54, pp. 561–590, AGU, Washington, D. C.
- MacIntyre, S., K. M. Flynn, R. Jellison, and J. Romero (1999), Boundary mixing and nutrient fluxes in Mono Lake, California, *Limnol. Oceanogr.*, *44*, 512–529, doi:10.4319/lo.1999.44.3.0512.
- MacIntyre, S., A. Jonsson, M. Jansson, J. Aberg, D. E. Turney, and S. D. Miller (2010), Buoyancy flux, turbulence, and the gas transfer coefficient in a stratified lake, *Geophys. Res. Lett.*, *37*, L24604, doi:10.1029/2010GL044164.
- Manasypov, R. M., O. S. Pokrovsky, S. N. Kirpotin, and L. S. Shirokova (2014), Thermokarst lake waters across the permafrost zones of western Siberia, *Cryosphere*, *8*, 1177–1193, doi:10.5194/tc-8-1177-2014.
- Manasypov, R. M., et al. (2015), Seasonal dynamics of organic carbon and metals in thermokarst lakes from the discontinuous permafrost zone of western Siberia, *Biogeosciences*, *12*, 3009–3028, doi:10.5194/bg-12-3009-2015.
- Manasypov, R. M., L. S. Shirokova, and O. S. Pokrovsky (2017), Experimental modeling of thaw lake water evolution in discontinuous permafrost zone: Role of peat, lichen leaching and ground fire, *Sci. Total Environ.*, *580*, 245–257.
- Markfort, C. D., A. L. S. Perez, J. W. Thill, D. A. Jaster, F. Porté-Agel, and H. G. Stefan (2010), Wind sheltering of a lake by a tree canopy or bluff topography, *Water Resour. Res.*, *46*, W03530, doi:10.1029/2009WR007759.
- Martinez-Cruz, K., A. Sepulveda-Jauregui, K. Walter Anthony, and F. Thalasso (2015), Geographic and seasonal variation of dissolved methane and aerobic methane oxidation in Alaskan lakes, *Biogeosciences*, *12*, 4595–4606, doi:10.5194/bg-12-4595-2015.
- Marushchak, M. E., I. Kiepe, C. Biasi, V. Elsakov, T. Friborg, T. Johansson, H. Soegaard, T. Virtanen, and P. J. Martikainen (2013), Carbon dioxide balance of subarctic tundra from plot to regional scales, *Biogeosciences*, *10*, 437–452, doi:10.5194/bg-10-437-2013.

- Molot, L. A., and P. J. Dillon (1996), Storage of terrestrial carbon in boreal lake sediments and evasion to the atmosphere, *Global Biogeochem. Cycles*, *10*, 483–492, doi:10.1029/96GB01666.
- Monteith, D. T., et al. (2007), Dissolved organic carbon trends resulting from changes in atmospheric deposition chemistry, *Nature*, *450*, 537–540.
- Morris, M. D. (1991), Factorial sampling plans for preliminary computational experiments, *Technometrics*, *33*, 161–174.
- Obernosterer, I., and R. Benner (2004), Competition between biological and photochemical processes in the mineralization of dissolved organic carbon, *Limnol. Oceanogr.*, *49*, 117–124, doi:10.4319/lo.2004.49.1.0117.
- Ohmura, A., et al. (1998), Baseline Surface Radiation Network (BSRN/WCRP): New precision radiometry for climate research, *Bull. Am. Meteorol. Soc.*, *79*, 2115–2136.
- O'Reilly, C. M., et al. (2015), Rapid and highly variable warming of lake surface waters around the globe, *Geophys. Res. Lett.*, *42*, 10,773–10,781, doi:10.1002/2015GL066235.
- Paltan, H., J. Dash, and M. Edwards (2015), A refined mapping of Arctic lakes using Landsat imagery, *Int. J. Remote Sens.*, *36*, 5970–5982, doi:10.1080/01431161.2015.1110263.
- Paytan, A., A. L. Lecher, N. Dimova, K. J. Sparrow, F. G.-T. Kodovska, J. Murray, S. Tulaczyk, and J. D. Kessler (2015), Methane transport from the active layer to lakes in the Arctic using Toolik Lake, Alaska, as a case study, *Proc. Natl. Acad. Sci. U. S. A.*, *112*(12), 3636–3640.
- Podgrajsek, E., E. Sahlée, and A. Rutgersson (2015), Diel cycle of lake-air CO₂ flux from a shallow lake and the impact of waterside convection on the transfer velocity, *J. Geophys. Res. Biogeosci.*, *120*, 29–38, doi:10.1002/2014JG002781.
- Prater, C., P. C. Frost, E. T. Howell, S. B. Watson, A. Zastepa, S. S. E. King, R. J. Vogt, and M. A. Xenopoulos (2017), Variation in particulate C:N:P stoichiometry across the Lake Erie watershed from tributaries to its outflow, *Limnol. Oceanogr.*, doi:10.1002/lno.10628, in press.
- Repo, M. E., J. T. Huttunen, A. V. Naumov, A. V. Chichulin, E. D. Lapshina, W. Bleuten, and P. J. Martikainen (2007), Release of CO₂ and CH₄ from small wetland lakes in western Siberia, *Tellus, Ser. B*, *59*, 788–796, doi:10.1111/j.1600-0889.2007.00301.x.
- Roulet, N., and T. R. Moore (2006), Browning the waters, *Nature*, *444*, 283–284.
- Rousseaux, C. S., and W. W. Gregg (2015), Recent decadal trends in global phytoplankton composition, *Global Biogeochem. Cycles*, *29*, 1674–1688, doi:10.1002/2015GB005139.
- Saloranta, T. M., and T. Andersen (2007), MyLake-A multi-year lake simulation model code suitable for uncertainty and sensitivity analysis simulations, *Ecol. Modell.*, *207*, 45–60, doi:10.1016/j.ecolmodel.2007.03.018.
- Saltelli, A., K. Chan, and E. M. Scott (2000), *Sensitivity Analysis*, John Wiley, New York.
- Saltelli, A., P. Annoni, I. Azzini, F. Campolongo, M. Ratto, and S. Tarantola (2010), Variance based sensitivity analysis of model output. Design and estimator for the total sensitivity index, *Comput. Phys. Commun.*, *181*, 259–270.
- Sayer, A. M., N. C. Hsu, C. Bettenhausen, Z. Ahmad, B. N. Holben, A. Smirnov, G. E. Thomas, and J. Zhang (2012), SeaWiFS Ocean Aerosol Retrieval (SOAR): Algorithm, validation, and comparison with other data sets, *J. Geophys. Res.*, *117*, D03206, doi:10.1029/2011JD016599.
- Schirmeister, L., G. Grosse, S. Wetterich, P. P. Overduin, J. Strauss, E. A. G. Schuur, and H. Hubberten (2011), Fossil organic matter characteristics in permafrost deposits of the northeast Siberian Arctic, *J. Geophys. Res.*, *116*, G00M02, doi:10.1029/2011JG001647.
- Schwanghart, W., and N. J. Kuhn (2010), TopoToolbox: A set of Matlab functions for topographic analysis, *Environ. Modell. Software*, *25*, 770–781, doi:10.1016/j.envsoft.2009.12.002.
- Seekell, D. A., J.-F. Lapierre, J. Ask, A.-K. Bergström, A. Deiningner, P. Rodríguez, and J. Karlsson (2015), The influence of dissolved organic carbon on primary production in northern lakes, *Limnol. Oceanogr.*, *60*, 1276–1285, doi:10.1002/lno.10096.
- Sepulveda-Jauregui, A., K. M. Walter Anthony, K. Martinez-Cruz, S. Greene, and F. Thalasso (2015), Methane and carbon dioxide emissions from 40 lakes along a north–south latitudinal transect in Alaska, *Biogeosciences*, *12*, 3197–3223, doi:10.5194/bg-12-3197-2015.
- Sheath, R. G. (1986), Seasonality of phytoplankton in northern tundra ponds, *Hydrobiologia*, *138*, 75–83.
- Sheffield, J., and E. F. Wood (2007), Characteristics of global and regional drought, 1950–2000: Analysis of soil moisture data from off-line simulation of the terrestrial hydrologic cycle, *J. Geophys. Res.*, *112*, D17115, doi:10.1029/2006JD008288.
- Shirokova, L. S., O. S. Pokrovsky, S. N. Kirpotin, C. Desmukh, B. G. Pokrovsky, S. Audry, and J. Viers (2013), Biogeochemistry of organic carbon, CO₂, CH₄, and trace elements in thermokarst water bodies in discontinuous permafrost zones of Western Siberia, *Biogeochemistry*, *113*, 573–593, doi:10.1007/s10533-012-9790-4.
- Sobek, S., E. Durisch-Kaiser, R. Zurbrügg, N. Wongfun, M. Wessels, N. Pasche, and B. Wehrli (2009), Organic carbon burial efficiency in lake sediments controlled by oxygen exposure time and sediment source, *Limnol. Oceanogr.*, *54*, 2243–2254, doi:10.4319/lo.2009.54.6.2243.
- Sobek, S., N. J. Anderson, S. M. Bernasconi, and T. Del Sontro (2014), Low organic carbon burial efficiency in Arctic lake sediments, *J. Geophys. Res. Biogeosci.*, *119*, 1231–1243, doi:10.1002/2014JG002612.
- Sobol, I. M. (1993), Sensitivity analysis for non-linear mathematical models, *Math. Modell. Comput. Exp.*, *1*, 407–414.
- Spencer, R. G. M., P. J. Mann, T. Dittmar, T. I. Eglinton, C. McIntyre, R. M. Holmes, N. Zimov, and A. Stubbins (2015), Detecting the signature of permafrost thaw in Arctic rivers, *Geophys. Res. Lett.*, *42*, 2830–2835, doi:10.1002/2015GL063498.
- Stackpoole, S. M., D. E. Butman, D. W. Clow, K. L. Verdin, B. V. Gaglioti, H. Genet, and R. G. Striegl (2017), Inland waters and their role in the carbon cycle of Alaska, *Ecol. Appl.*, *27*(5), 1403–1420, doi:10.1002/eap.1552.
- Stepanenko, V., I. Mammarella, A. Ojala, H. Miettinen, V. Lykosov, and T. Vesala (2016), LAKE 2.0: A model for temperature, methane, carbon dioxide and oxygen dynamics in lakes, *Geosci. Model Dev.*, *9*, 1977–2006, doi:10.5194/gmd-1977-2016.
- Stubbins, A., P. J. Mann, L. Powers, T. B. Bittar, T. Dittmar, C. McIntyre, T. I. Eglinton, N. Zimov, and R. G. M. Spencer (2017), Low photolability of yedoma permafrost dissolved organic carbon, *J. Geophys. Res. Biogeosci.*, *122*, 200–211, doi:10.1002/2016JG003688.
- Subin, Z. M., W. J. Riley, and D. Mironov (2012), An improved lake model for climate simulations: Model structure, evaluation, and sensitivity analyses in CESM1, *J. Adv. Model. Earth Syst.*, *4*, M02001, doi:10.1029/2011MS000072.
- Tan, Z., and Q. Zhuang (2015a), Arctic lakes are continuous methane sources to the atmosphere under warming conditions, *Environ. Res. Lett.*, *10*, 054016, doi:10.1088/1748-9326/10/5/054016.
- Tan, Z., and Q. Zhuang (2015b), Methane emissions from pan-Arctic lakes during the 21st century: An analysis with process-based models of lake evolution and biogeochemistry, *J. Geophys. Res. Biogeosci.*, *120*, 2641–2653, doi:10.1002/2015JG003184.
- Tan, Z., Q. Zhuang, and K. Walter Anthony (2015), Modeling methane emissions from Arctic lakes: Model development and site-level study, *J. Adv. Model. Earth Syst.*, *7*, 459–483, doi:10.1002/2014MS000344.
- Tan, Z., Q. Zhuang, D. K. Henze, C. Frankenberg, E. Dlugokencky, C. Sweeney, A. J. Turner, M. Sasakawa, and T. Machida (2016), Inverse modeling of pan-Arctic methane emissions at high spatial resolution: What can we learn from assimilating satellite retrievals and using different process-based wetland and lake biogeochemical models?, *Atmos. Chem. Phys.*, *16*, 12,649–12,666, doi:10.5194/acp-16-12649-2016.
- Tang, J., and Q. Zhuang (2009), A global sensitivity analysis and Bayesian inference framework for improving the parameter estimation and prediction of a process-based Terrestrial Ecosystem Model, *J. Geophys. Res.*, *114*, D15303, doi:10.1029/2009JD011724.

- Tang, J., Q. Zhuang, R. D. Shannon, and J. R. White (2010), Quantifying wetland methane emissions with process-based models of different complexities, *Biogeosciences*, *7*(11), 3817–3837, doi:10.5194/bg-7-3817-2010.
- Tarnocai, C., J. G. Canadell, E. A. G. Schuur, P. Kuhry, G. Mazhitova, and S. Zimov (2009), Soil organic carbon pools in the northern circumpolar permafrost region, *Global Biogeochem. Cycles*, *23*, GB2023, doi:10.1029/2008GB003327.
- Tian, R. C. (2006), Toward standard parameterizations in marine biological modeling, *Ecol. Modell.*, *193*, 363–386, doi:10.1016/j.ecolmodel.2005.09.003.
- Tranvik, L., et al. (2009), Lakes and reservoirs as regulators of carbon cycling and climate, *Limnol. Oceanogr.*, *54*, 2298–2314.
- Treat, C., et al. (2015), A pan-Arctic synthesis of CH₄ and CO₂ production from anoxic soil incubations, *Global Change Biol.*, *21*, 2787–2803, doi:10.1111/gcb.12875.
- Trenberth, K. E., J. T. Fasullo, and J. Kiehl (2009), Earth's global energy budget, *Bull. Am. Meteorol. Soc.*, *90*, 311–323.
- Vachon, D., Y. T. Prairie, F. Guillemette, and P. A. del Giorgio (2017), Modeling allochthonous dissolved organic carbon mineralization under variable hydrologic regimes in boreal lakes, *Ecosystems*, *20*, 781–795, doi:10.1007/s10021-016-0057-0.
- van der A, R. J., M. A. F. Allaart, and H. J. Eskes (2010), Multi sensor reanalysis of total ozone, *Atmos. Chem. Phys.*, *10*, 11,277–11,294.
- Verpoorter, C., T. Kutser, D. A. Seekell, and L. J. Tranvik (2014), A global inventory of lakes based on high-resolution satellite imagery, *Geophys. Res. Lett.*, *41*, 6396–6402, doi:10.1002/2014GL060641.
- von Wachenfeldt, E., and L. J. Tranvik (2008), Sedimentation in boreal lakes—The role of flocculation of allochthonous dissolved organic matter in the water column, *Ecosystems*, *11*, 803–814, doi:10.1007/s10021-008-9162-z.
- Vonk, J. E., et al. (2013), High biolability of ancient permafrost carbon upon thaw, *Geophys. Res. Lett.*, *40*, 2689–2693, doi:10.1002/grl.50348.
- Walter, K. M., S. A. Zimov, J. P. Chanton, D. Verbyla, and F. S. Chapin III (2006), Methane bubbling from Siberian thaw lakes as a positive feedback to climate warming, *Nature*, *443*, 71–75, doi:10.1038/nature05040.
- Walter Anthony, K. M., et al. (2014), A shift of thermokarst lakes from carbon sources to sinks during the Holocene epoch, *Nature*, *511*, 452–456, doi:10.1038/nature13560.
- Wang, X. J., M. Behrenfeld, R. Le Borgne, R. Murtugudde, and E. Boss (2009), Regulation of phytoplankton carbon to chlorophyll ratio by light, nutrients and temperature in the equatorial Pacific Ocean: A basin-scale model, *Biogeosciences*, *6*, 391–404, doi:10.5194/bg-6-391-2009.
- Ward, C. P., and R. M. Cory (2016), Complete and partial photo-oxidation of dissolved organic matter draining permafrost soils, *Environ. Sci. Technol.*, *50*, 3545–3553, doi:10.1021/acs.est.5b05354.
- Ward, N. D., T. S. Bianchi, P. M. Medeiros, M. Seidel, J. Richey, R. G. Keil, and H. O. Sawakuchi (2017), Where carbon goes when water flows: Carbon cycling across the aquatic continuum, *Front. Mar. Sci.*, *4*, 7, doi:10.3389/fmars.2017.00007.
- Wetzel, R. G. (2001), *Limnology*, 3rd ed., Academic, San Diego, Calif.
- Weyhenmeyer, G. A., M. Fröberg, E. Karlton, M. Khalili, D. Kothawala, J. Temnerud, and L. J. Tranvik (2012), Selective decay of terrestrial organic carbon during transport from land to sea, *Global Change Biol.*, *18*, 349–355, doi:10.1111/j.1365-2486.2011.02544.x.
- Wik, M., R. K. Varner, K. W. Anthony, S. MacIntyre, and D. Bastviken (2016), Climate-sensitive northern lakes and ponds are critical components of methane release, *Nat. Geosci.*, *9*, 99–105, doi:10.1038/ngeo2578.
- Wüest, A., N. H. Brooks, and D. M. Imboden (1992), Bubble plume modeling for lake restoration, *Water Resour. Res.*, *28*, 3235–3250.
- Zhuang, Q., et al. (2003), Carbon cycling in extratropical terrestrial ecosystems of the Northern Hemisphere during the 20th Century: A modeling analysis of the influences of soil thermal dynamics, *Tellus, Ser. B*, *55*, 751–776.
- Zhuang, Q., J. He, Y. Lu, L. Ji, J. Xiao, and T. Luo (2010), Carbon dynamics of terrestrial ecosystems on the Tibetan Plateau during the 20th century: An analysis with a process-based biogeochemical mode, *Global Ecol. Biogeogr.*, *19*, 649–662, doi:10.1111/j.1466-8238.2010.00559.x.